

~~CONFIDENTIAL~~
UNCLASSIFIED

Copy 147
RM L51K23

NACA RM L51K23



RESEARCH MEMORANDUM

THE INTERFERENCE EFFECTS OF A BODY ON THE SPANWISE LOAD
DISTRIBUTIONS OF TWO 45° SWEEPBACK WINGS OF ASPECT
RATIO 8 FROM LOW-SPEED TESTS AT A REYNOLDS
NUMBER OF 4×10^6

By Albert P. Martina

Langley Aeronautical Laboratory
Langley Field, Va.

CLASSIFICATION CHANGE

To **UNCLASSIFIED**
By Authority of *J.W. Crowley per NACA Rel. Form 2695, 10-12-54*
Changed by *skm* Date *4-28*

CLASSIFIED DOCUMENT

This material contains information affecting the National Defense of the United States within the meaning of the espionage laws, Title 18, U.S.C., Secs. 793 and 794, the transmission or revelation of which in any manner to unauthorized person is prohibited by law.

NATIONAL ADVISORY COMMITTEE FOR AERONAUTICS

WASHINGTON
February 26, 1952

~~CONFIDENTIAL~~
UNCLASSIFIED



NATIONAL ADVISORY COMMITTEE FOR AERONAUTICS

RESEARCH MEMORANDUM

THE INTERFERENCE EFFECTS OF A BODY ON THE SPANWISE LOAD

DISTRIBUTIONS OF TWO 45° SWEEPBACK WINGS OF ASPECT

RATIO 8 FROM LOW-SPEED TESTS AT A REYNOLDS

NUMBER OF 4×10^6

By Albert P. Martina

SUMMARY

Tests of two wing-body combinations have been conducted in the Langley 19-foot pressure tunnel at a Reynolds number of 4×10^6 and a Mach number of 0.19 to determine the effects of the bodies on the wing span load distributions. The wings had 45° sweepback of the quarter-chord line, aspect ratio 8.02, taper ratio 0.45, and incorporated 12-percent-thick NACA 63A-series airfoil sections in the streamwise direction. One wing was untwisted and uncambered while the second wing incorporated both twist and camber. Identical bodies of revolution, both of fineness ratio 10, having maximum diameters of 10 percent of the wing spans, were mounted in mid-high-wing arrangements. The effects on the incremental loading due to the body resulting from wing incidence, upper-surface wing fences, and flap deflection were determined for the plane uncambered wing.

The addition of the body to the plane wing increased the exposed wing loading at a given lift coefficient as much as 10 percent with the body at 0° incidence and 4 percent at 4° incidence. The body-induced lift disappeared near maximum lift in both cases. The bending-moment coefficients at the wing-body juncture were increased about 2 percent with the body at 0° incidence; whereas the increases were as much as 10 percent with the body at 4° incidence. In both cases the increases disappeared near maximum lift.

The spanwise load distributions due to the body on the plane wing as calculated by using a swept-wing method employing 19 spanwise lifting elements and control points generally showed satisfactory agreement with experiment whereas the distributions calculated by using the swept-wing method of NACA RM L51J19 displayed considerable underestimation of the body influence. The spanwise load distributions due to body on the flapped plane wing and on the twisted and cambered wing were dissimilar to those obtained on the plane wing. Neither of the methods

~~CONFIDENTIAL~~

UNCLASSIFIED

yielded distributions that agreed consistently with experiment for either the flapped plane wing or the twisted and cambered wing.

INTRODUCTION

Theoretical studies have shown that the effects of a body on the wing spanwise load distribution are dependent upon the angle of attack, the angle of incidence between the wing and body, the cross-sectional shape and size of the body, the vertical position of the wing on the body, and on the forebody length in cases where the length is extremely short. Experimental data showing these effects are relatively meager. The results of an investigation which shows the variation of body effects with wing vertical position on an unswept wing are reported in reference 1. Results of investigations made to show the body effects on two sweptback wing-body combinations for one vertical wing position are given in references 2, 3, and 4. All of these investigations were carried out in the low-to-moderate lift-coefficient range at low speed.

Several investigators have undertaken the calculation of the body effect on both unswept wings (references 5 to 9) and on swept wings (references 10 to 12), although practically no direct experimental verifications of these methods are available.

Consequently, an investigation was conducted in the Langley 19-foot pressure tunnel to determine the body effects on the spanwise load distributions of two sweptback wings and to determine whether the body effects could be estimated through the use of existing methods. The wings were similar in plan form, one was plane and uncambered while the second was twisted and cambered for a design lift coefficient of 0.7. The investigation was made for one vertical position of the wings on the body. The influence on the body effects of incidence, of upper-surface wing fences, and flap deflection were investigated on the plane wing. Results of other investigations on the plane uncambered wing are reported in references 13 to 16.

COEFFICIENTS AND SYMBOLS

The data are referred to the wind axes the origin of which is located in the plane of symmetry at 25 percent of the wing mean aerodynamic chord. Standard NACA coefficients and symbols are used throughout and are defined as follows:

~~CONFIDENTIAL~~

UNCLASSIFIED

- C_L lift coefficient $\left(\frac{\text{Lift}}{qS_w} \text{ or } \int_0^{1.0} c_{l, \frac{c}{c}} d\left(\frac{y}{b/2}\right) \right)$
- c_l section lift coefficient $(c_n \cos(\alpha + \epsilon) - c_c \sin(\alpha + \epsilon))$
- c_n section normal-force coefficient $\left(\int_0^{1.0} (S_u - S_l) d\left(\frac{x}{c}\right) \right)$
- c_c section chord-force coefficient $\left(\int_{-(z/c)_{\max}}^{(z/c)_{\max}} (S_r - S_f) d\left(\frac{z}{c}\right) \right)$
- C_b exposed wing-root bending-moment coefficient

$$\left(\frac{1}{c} \int_{0.10}^{1.0} c \left[c_n \cos(\epsilon - \epsilon_{0.10b/2}) + c_c \sin(\epsilon - \epsilon_{0.10b/2}) \right] \left[\frac{y}{b/2} - 0.10 \right] d\left(\frac{y}{b/2}\right) \right)$$
- S pressure coefficient $\left(\frac{H - P}{q} \right)$
- R Reynolds number $\left(\frac{\rho V c'}{\mu} \right)$
- μ coefficient of viscosity of air
- x longitudinal coordinate from local leading edge parallel to local chord line
- y lateral coordinate perpendicular to plane of symmetry
- z vertical coordinate normal to local chord line
- \bar{x} longitudinal center of pressure of exposed wing load normal to chord at $0.10b/2$ measured from $0.25c'$ and parallel to chord at $0.10b/2$
- \bar{y} lateral center of pressure of exposed wing load normal to chord at $0.10b/2$ measured perpendicular to plane of symmetry

S_w	wing area
c	local chord
c'	mean aerodynamic chord $\left(\frac{2}{S_w} \int_0^{1.0} c^2 d\left(\frac{y}{b/2}\right) \right)$
\bar{c}	mean geometric chord $\left(\frac{S_w}{b} \right)$
b	wing span
H	free-stream total pressure
p	local static pressure
q	dynamic pressure $\left(\frac{\rho V^2}{2} \right)$
ρ	mass density of air
V	free-stream velocity
α	angle of attack of root chord
ϵ	geometric angle of twist of any section referred to the plane of symmetry (negative if washout)
i_w	angle of incidence, angle between wing-root chord and the axis of body (positive if angle of attack of root-section is greater than that of body)
Δ	incremental value
Subscripts:	
u	upper surface
l	lower surface
f	forward of maximum thickness
r	rearward of maximum thickness
o	zero lift

s section at plane of symmetry
max maximum
e effective

MODEL AND APPARATUS

The two wings in this investigation had 45° sweepback of the 25-percent-chord line, aspect ratio 8.02, and taper ratio 0.45. Further details are given in figure 1. The wings were of composite construction, each consisting of a solid steel core upon which was bonded a layer of 50-percent bismuth and 50-percent tin alloy. The surfaces were machined and finished to aerodynamically smooth contours which were so maintained throughout the periods of testing. One wing was untwisted and incorporated NACA 63₁A012 airfoil sections in the streamwise direction. The second wing embodied NACA 63₁A012 thickness distributions in the streamwise direction but was cambered and twisted according to the variations shown in figure 2. The mean camber line, which is described in table I, was a slightly modified $a = 1.0$ mean line. The wing sections were twisted about the 80-percent chord line; hence this line had no dihedral.

The flap configuration which was investigated on the plane wing is shown in figure 3. All of the flaps were constructed of steel and were mounted by means of steel angle blocks in the case of the trailing-edge flaps and by means of wooden blocks in the case of the leading-edge flaps (fig. 3, section A-A). The latter mounting was used to avoid damaging the wing contour near the leading edge. The upper-surface fences used on the plane wing, which are shown in figure 1, were made of sheet steel and were attached to the wing by means of angle brackets located on the outboard sides of the fences.

The bodies of revolution used in these tests were identical, having constant diameter central sections joining the elliptic forebodies and parabolic afterbodies (fig. 1). The bodies, which were constructed of laminated mahogany, had fineness ratios of 10, and maximum diameters of 10 percent of the wing spans. The wings were mounted in mid-high-wing arrangements with the wing-root chords set at zero incidence with respect to the body axes. An additional incidence angle of 4° was tested on the plane wing with the leading edge of the root chord maintained at the same vertical position from the body axis as for zero incidence (fig. 1).

TESTS

The tests reported herein were conducted in the Langley 19-foot pressure tunnel at a pressure of approximately $2\frac{1}{3}$ atmospheres. All tests were conducted at a Reynolds number of 4.0×10^6 , which corresponds to values of dynamic pressure, and Mach number of approximately 125 pounds per square foot and 0.19, respectively.

Force measurements were obtained for an angle-of-attack range from -3.5° to 31° by means of simultaneous recording balances. Pressure measurements, which were made independently of force measurements, were recorded by photographing multitube tunnel manometers and thus all the pressures were recorded simultaneously. The pressure data were reduced to coefficient form by means of an NACA combination film reader and computer.

Pressure-distribution measurements were made over the left wing of each model by means of surface orifices located spanwise, as shown in figure 4, and chordwise, as indicated in table II. The orifices were formed from 0.040-inch monel tubing embedded in the bismuth-tin layer. The tubes connecting the orifices to the tunnel manometers were conducted from each model through a tube transfer fairing located at 20.4 percent of the right wing span on the lower wing surface, as seen in figure 5. Not only were the effects of these fairings upon the orifice stations at the planes of symmetry believed to be negligible, but preliminary tests showed that their effects upon the wing characteristics were negligible. As seen in table II, the orifice stations at 0.03b/2 on the wings were incomplete; consequently, additional measurements were made by means of a static-pressure survey tube maintained approximately 0.0035c from the wing contours and alined as nearly as possible with the local flow.

Since reductions in loading occur near the wing-body junctures, additional measurements were made in an attempt to obtain loadings at spanwise stations that were outside the immediate influence of the junctures. These additional measurements were made at 0.15b/2. Upper-surface pressures on the plane wing were measured by means of orifices located in a multitube plastic tape that was cemented to the wing surface. No pressures were measured on the lower surface inasmuch as a fairly accurate interpolation of the lower-surface loading was made possible by the small variation of the lower-surface loading between the 10- and 30-percent semispan orifice stations. It was only possible to make these additional measurements for the wing-body combination having 4° wing incidence. On the twisted and cambered wing, the additional pressure measurements were made by means of a copper tube belt attached to both

the upper and lower surfaces. The measurements were made with and without the body at zero incidence.

With the body present, no flap pressures were measured at the 0.10b/2 station. Inasmuch as the lower-surface pressures at 0.10b/2 with body were almost identical to the lower-surface pressures at the plane of symmetry without body, the flap pressures at 0.10b/2 with body were assumed to be the same as those at the plane of symmetry without body.

CORRECTIONS TO DATA

All force data were corrected for support tares and interference and for air-stream misalignment. The jet-boundary correction to the angle of attack was determined by means of reference 17 and was as follows:

$$\Delta\alpha = 0.387C_L$$

The jet-boundary correction to the angle of attack applied to the results obtained from pressure-distribution measurements was the same as that applied to the force data. No corrections were applied to take into account the spanwise variation of the jet-boundary-induced angle or the model twist due to air load. Calculations of the induced angles and measurements of the plane wing twist due to air load indicated that the variations of these angles between the root and tip not only were small and of the same order of magnitude (0.2° at $C_L = 1.0$) but were opposite in sign and thus tended to cancel each other so that the resultant variation was negligible.

The spanwise load distributions obtained from integrations of the chordwise pressure-distribution data were corrected for a spanwise variation of stream angle and, in the case of the plane wing, for model and experimental inaccuracies, as explained in reference 13. The lift distribution applied to the results for the configurations with the plane wing is given in figure 6(a) and was determined from the experimental section-loading curves. The lift distribution applied to the results for the configurations with the twisted and cambered wing is given in figure 6(b) and was calculated from the results of air-stream surveys, as indicated in reference 13.

RESULTS AND DISCUSSION .

The addition of a body to a wing alters the loading at a given wing section as a result of the body-induced angle of attack which arises from the flow component normal to the longitudinal axis of the body. The incremental loading, when separated into components due to angle of attack and to angle of incidence (as was done in reference 8), can be expressed thusly:

$$\Delta c_l \frac{c}{c} = \Delta c_{l_0} \frac{c}{c} + \alpha_e \frac{\partial}{\partial \alpha} \left(c_l \frac{c}{c} \right) + i_{w_e} \frac{\partial}{\partial i_w} \left(c_l \frac{c}{c} \right) \quad (1)$$

where

$$\Delta c_{l_0} \frac{c}{c} = \left(c_l \frac{c}{c} \right)_{\text{wing-body}} - \left(c_l \frac{c}{c} \right)_{\text{wing}} \quad \text{at } \alpha_{0_S} \quad \text{and } i_w = 0 \quad (2)$$

the incremental section basic loading due to wing vertical position on body (asymmetry);

$$\alpha_e \frac{\partial}{\partial \alpha} \left(c_l \frac{c}{c} \right) = \left(c_l \frac{c}{c} \right)_{\text{wing-body}} - \left(c_l \frac{c}{c} \right)_{\text{wing}} \quad \text{at } \alpha = \text{const.} \quad (3)$$

the incremental section loading due to angle of attack;

$$i_{w_e} \frac{\partial}{\partial i_w} \left(c_l \frac{c}{c} \right) = \left(c_l \frac{c}{c} \right)_{i_w} - \left(c_l \frac{c}{c} \right)_{i_w=0} \quad \text{at } \alpha = \text{const.} \quad (4)$$

the incremental change in section loading due to a change in wing incidence;

and,

$$\alpha_e = \alpha - \alpha_{0_S}, \quad \text{the effective angle of attack} \quad (5)$$

$$i_{w_e} = i_w - \alpha_{0_S}, \quad \text{the effective angle of incidence} \quad (6)$$

Span Load Due to Angle of Attack for Plane Wing

The body effects upon the wing span load distribution are clearly perceptible as far outboard as the 90-percent semispan station in the moderate lift coefficient range, as seen in figure 7. Aside from increases in the section lift-curve slopes in the linear lift range, it appears from the data of figure 8 that the body caused no significant changes to the section characteristics. The body effects on the section loading became inconsistent as each section reached maximum lift. The analysis of body effects, consequently, generally includes only angles of attack up to 12.9° inasmuch as many of the wing sections were operating near or beyond maximum lift above this angle of attack.

A comparison is presented in figure 9 between the calculated and experimental slopes of the incremental loading curves; that is, the derivative in the second term of equation (1), and in figure 10 between the calculated and experimental loading increments for several angles of attack. The calculated values were obtained by using an unswept-wing method (reference 8) and two swept-wing methods; namely, that of reference 11 and a method hereinafter referred to as the 19×1 method which is described in appendices A and B. In the 19×1 method, the body effect is treated as a twist distribution and the calculations are carried out directly for the actual wing. The distribution of lifting elements and control points (19 each) used in this 19×1 method was shown in reference 14 to define accurately the loading on this wing and, furthermore, would be considered the minimum number for taking into account the body effects. In applying the method of reference 11, the calculations were made as outlined therein with the exception of the inflow correction to the span load δ which accounts for some of the increase in velocity about the body. This factor δ , as applied herein, was computed by means of the equations given in reference 18 at the maximum diameter of an ellipsoid of 10:1 fineness ratio. The span load calculated by this method is somewhat too large because the correction factor δ , based on an ellipsoid is larger than for the actual body used in these tests. This fact can be seen in reference 19 by comparing the induced axial velocity $\frac{-v_x}{U}$ on the surface at the midpoint of an ellipsoid of fineness ratio 10:1 with that at 0.32 of the length (corresponding to the wing leading edge at the juncture) of the nearly cylindrical body with rounded nose and pointed tail having the same fineness ratio. In the case of the nearly cylindrical body, which is almost exactly similar to the body used in these tests, $\delta = 0.017$, whereas $\delta = 0.021$ for the ellipsoid. The calculations necessary to obtain the spanwise variation of the factor δ for the exact body were deemed too lengthy for the additional refinement that would be gained here. The values calculated by means of the 19×1 method and shown in figures 9 and 10 agree satisfactorily with experiment both in magnitude and

in the manner of variation, except near the wing-body juncture where the calculated values substantially exceeded the experimental values. The values calculated by means of reference 11, however, show some agreement at the juncture but considerably underestimated the body effects over the remainder of the span. It is of interest to note in figure 9 that the body effects on the spanwise loading calculated for an unswept wing of the same aspect and taper ratios as the wing of the present tests using the method of reference 8 are nearly identical to those calculated by the 19×1 method. This result tends to indicate, at least theoretically, that for this case sweep has second-order effects on the body influence, which may result from the high aspect ratio. Since a comparatively small depression in the loading over the body width is implicit in the 19×1 method of calculation, some overestimation is to be expected inasmuch as the loading over the equivalent wing area covered by the body is greatly reduced. In this case, the loading at the plane of symmetry was one-half the wing-alone value at the plane of symmetry. Preliminary calculations in which a reduced lift-curve slope at the plane of symmetry was used indicated that the calculated values of the body-induced loading near the juncture were more nearly in agreement with the experimental trends. These calculations were carried out by using the 19×1 method, but it is believed that a greater number of spanwise points would be necessary to define the discontinuity in the loading. It thus appears highly probable that the use of the 19×1 method without making allowance for the reduced lift-curve slopes over the body width will result in overestimates of the loading in the proximity of the wing-body juncture for any configuration. Additional overestimation in the total increments (fig. 10) arises from the fact that a positive shift in the angle of zero lift occurs at the 10-percent semispan station from adding the body, a shift which most methods of calculation cannot take into account.

The shift in the angle of zero lift at the 10-percent semispan station is attributable to the asymmetrical vertical position of the wing on the body and is in agreement with the trends indicated by the results of reference 20. In the realm of influence of the wing-body juncture, only a midwing position having zero wing incidence would experience no change in the angle of zero lift for this wing-body combination since the upper- and lower-surface pressure distributions would then be identical at zero lift.

Further insight into the angle shift can be had by making comparisons between the chordwise pressure distributions at the 10-percent semispan station with and without body and with the plane of symmetry station as done in figure 11. These distributions are all at $\alpha = 0.6^\circ$. It can be seen in figure 11(b) that the body nearly effects a full reflection of the flow on the lower surface since the pressure distribution at 10-percent semispan agrees quite closely with that at the plane of symmetry, body off. The differences that do exist arise from the shape of the wing-body juncture. The upper-surface pressure distribution, however, lies

between the pressure distributions at the plane of symmetry and that at 10-percent semispan, body off (fig. 11(a)). This result can be ascribed to the wing position on the body which, because of the small body thickness above the wing, affects only a partial reflection of the type of flow found at the plane of symmetry. In addition, there are localized juncture effects which tend to reduce the wing-alone velocities over the forward part of the section and increase the velocities over the rear part. These velocity changes which were produced by adding the body result in a down load over the rear half of the section, as shown in figure 12, which obviously reduces the section loading and shifts the angle of zero lift positively.

Since the addition of upper-surface fences significantly altered the wing-span load distribution at moderate angles of attack, the influence of the body was determined for this configuration. The variations of the section loadings with angle of attack are presented in figure 13, and the incremental span load distributions for several angles are presented in figure 14 and compared with those for the wing without fences. As a result of delaying separation over the tip sections, it can be seen in figure 14(c) that the addition of fences caused the body effect to be increased over the tip sections at $\alpha = 16.0^\circ$ with no significant changes indicated in the incremental loadings over the inboard sections. The low value at the 55-percent semispan station at this angle results from the fact that this section stalled earlier on the wing with fences than it did on the wing without fences.

Span Load Due to Wing Incidence for Plane Wing

The effects on the span load distributions of changing the wing incidence are shown in figure 15 and on the variations of the load coefficients with angle of attack in figure 16. No apparent slope changes resulted from changing the wing incidence (fig. 16) although the lift was reduced by the positive change in wing incidence. This reduced lift results from the fact that for positive incidence the body is always at a lower angle of attack than the wing, whereas at zero incidence the body is at the same angle of attack as the wing. The incremental changes in loading across the span are presented in figure 17(a) for several angles of attack together with the calculated variations. The calculated variations were obtained by using the same methods as in the preceding section. In general, similar results were obtained as at zero incidence in that the values calculated by using the 19×1 method showed good agreement with experiment at all points except at 30-percent semispan, whereas the method of reference 11 slightly underestimated the incidence effect over the entire span. It is of interest to note that the incidence effect (fig. 17(b)) is of opposite sign to the angle-of-attack effect (fig. 9) and is about $\frac{1}{2}$ times larger.

Span Load for Plane Wing with Leading-
and Trailing-Edge Flaps Deflected

The effects of adding a body to the wing with leading-edge and trailing-edge split flaps deflected are shown in figure 18. Aside from the large loss of lift at the 10-percent semispan station, no unusual interference effects were noted. Inasmuch as there were 4° geometric incidence between wing and body, in addition to the incidence produced by flap deflection, the reductions in lift which occurred with the addition of the body would be expected. In contrast to the results obtained on the unflapped wing where the maximum loading increases occurred near the body (fig. 19), the loading increases over the sections near the body with trailing-edge flaps deflected were less than one-half those obtained on the plane wing. Outboard of the 50-percent semispan station, the loading increases were as much as double those obtained on the unflapped wing.

The incremental loadings due to the addition of the body are presented in figure 20 for several angles of attack. Some of the increments, for example at $0.1Qb/2$, display practically no variation with angle of attack and confirm the small changes in lift-curve slopes previously noted. The calculated incremental loadings are also shown and were based on equation (1) by using an assumed $\alpha_{0g} = -11.1^\circ$ together with the respective derivatives obtained from the two methods of calculation (reference 11 and the 19×1 method). The loadings calculated by means of reference 11 showed fair agreement with experiment at all angles of attack, whereas the loadings calculated by using the 19×1 method showed fair agreement at the lowest angle of attack only. The disagreement at the higher angles resulted from the overprediction of the angle-of-attack effect.

Span Load for Twisted and Cambered Wing

The effects of the body on the variations of the section loadings with angle of attack are presented in figure 21. The increases in section lift-curve slopes near the body are less than half of those obtained on the plane wing, as shown in figure 22, and indicate that the amount of loading due to a change in angle of attack is less than one-half that produced on the plane wing, whereas outboard the increases were as much as doubled. The angle-of-attack effects on this twisted and cambered wing appear to be similar to those of the flapped wing (fig. 19). The incremental span load resulting from the addition of the body to the wing as shown in figure 23 for several angles of attack was rather small. The calculated incremental loadings are also shown and were based on equation (1) by using an assumed $\alpha_0 = -3.1^\circ$ together

with the respective derivatives obtained from the two methods of calculation (reference 11 and the 19×1 method). Neither of the methods yielded span load distributions that agreed consistently with experiment. This result tends to indicate that the large amount of camber used in this wing either compensates for and/or partly nullifies the flow component normal to the body axis such that the variation of the body-induced angle with angle of attack is greatly reduced. No explanation for this effect is readily apparent.

Over-All Effects of the Body-Induced Lift on the Wing-Body Combination

The body effects on the section loadings have been considered in the previous sections and now an evaluation of these effects in relation to the entire combination will be made. A spanwise integration of the body-induced loading (equation (1)) across the exposed wing yields the body-induced lift which affects not only the lift but all of those characteristics which are dependent on the span load distribution.

The magnitude and variation with angle of attack of the body-induced lift are shown in figure 24 along with the variations of body lift and the exposed wing lift for the combination having zero incidence. The exposed wing was taken as that part of the wing between 10- and 100-percent semispan, inasmuch as the trace of the wing-body juncture on the lower surface of the wing extended almost to the 10-percent station. The body-induced lift expressed as a fraction of the total lift is given in figure 25, from which it can be seen that it is comparatively small, never exceeding more than 10 percent of the total lift. This maximum value occurred in the low-lift-coefficient range, whereas the body-induced lift gradually diminished with increasing lift coefficient and disappeared at maximum lift ($\alpha \approx 21^\circ$). It is of interest to note that the body lift (fig. 24) was nearly the same as the lift carried by the same area on the wing without body except in the high-lift range.

The changes produced by the body effects on those characteristics which are dependent on the span load are illustrated in figure 26, wherein the changes to the bending-moment coefficients and to the longitudinal and spanwise centers of pressure are presented as functions of lift coefficient. The bending-moment coefficients (fig. 26(a)) at a given lift coefficient were increased an average of 2 percent of the exposed wing-alone bending moments throughout the lift-coefficient range for the case of zero incidence and gradually disappeared near maximum lift. The changes to the spanwise centers of pressure appeared to be comparatively small (fig. 26(b)) and amounted to an inward shift that reached a maximum of 4 percent of the wing semispan in the high-lift range. The longitudinal centers-of-pressure changes shown in figure 26(c) consisted of

forward shifts of the center of pressure which averaged about 4 percent of the wing mean aerodynamic chord.

The effects of increasing the wing incidence are shown by the dashed curves in figures 25 and 26. The effects of increased wing incidence were to reduce the relative amount of body-induced lift to a maximum of 4 percent which occurred in the high-lift range (fig. 25), although the body-induced lift disappeared at maximum lift as at zero incidence. The bending-moment coefficients at the wing-body juncture, however, were increased as much as 10 percent in the low-lift range (fig. 26(a)) since the wing carried a greater load at the higher incidence. The bending-moment increases disappeared at maximum lift.

CONCLUDING REMARKS

Tests at a Reynolds number of 4×10^6 of two wing-body combinations, one consisting of a plane uncambered wing and the other of a twisted and cambered wing, each having 45° sweepback and aspect ratio 8, and circular cross-section bodies of fineness ratio 10 with the wings mounted in mid-high-wing positions, have indicated the following results:

1. The addition of the body to the plane wing increased the exposed wing loading at given values of lift coefficient as much as 10 percent at 0° incidence and 4 percent at 4° incidence. The body-induced lift in both cases disappeared near maximum lift. The bending-moment coefficients at the wing-body junctures were increased about 2 percent with the body at 0° incidence, whereas at 4° incidence the increases were as much as 10 percent, although in both cases the increases disappeared near maximum lift. The changes in the spanwise centers of pressure were comparatively small and never exceeded an inboard shift of more than 4 percent of the wing-alone values. The longitudinal centers of pressure of the exposed wing were shifted forward an average of 4-percent wing mean aerodynamic chord.

2. Addition of the body to either the flapped plane wing or to the twisted and cambered wing produced increases in the section lift-curve slopes which over the inner 50-percent semispan were less than half the increases produced by adding the body to the plane wing, while over the outer 50-percent semispan the increases were as much as doubled.

3. The spanwise load distributions due to the body, as calculated by using a swept-wing method employing 19 spanwise lifting elements and control points agreed satisfactorily with experiment at all points except the wing-body juncture on the plane wing. The distributions due to the body, as calculated by using the swept-wing method of NACA RM L51J19 displayed fair agreement at the wing-body juncture but showed considerable

underestimation over the remainder of the span of the plane wing. The span load distributions due to the body on the flapped plane wing and on the twisted and cambered wing were dissimilar to those obtained on the plane wing. Neither of the methods yielded span load distributions that agreed consistently with experiment for either the flapped plane wing or the twisted and cambered wing.

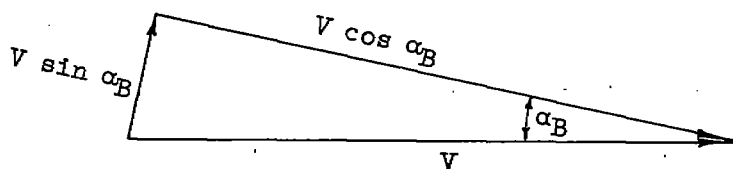
Langley Aeronautical Laboratory
National Advisory Committee for Aeronautics
- Langley Field, Va.

APPENDIX A

CALCULATION OF THE BODY-INDUCED ANGLE OF ATTACK

IN THE 19×1 METHOD

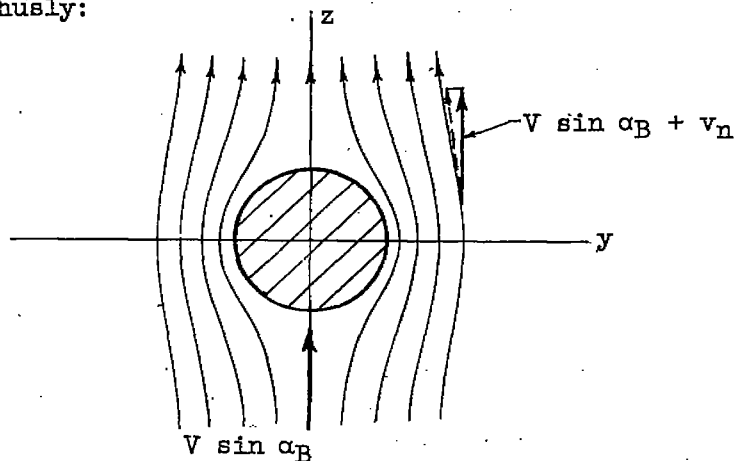
For the purposes of this calculation the body was assumed to be replaced by an infinite cylinder having the cross-sectional shape of the body used in these tests. With the cylinder at an angle of attack, the following velocity components, perpendicular and parallel to the cylinder axis can be written in terms of the free-stream velocity:



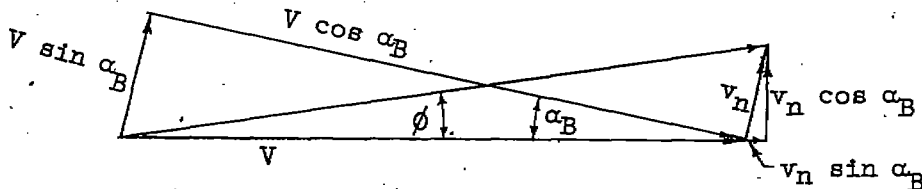
where

- V free-stream velocity
 α_B angle of attack of body
 $V \cos \alpha_B$ velocity component parallel to body axis
 $V \sin \alpha_B$ velocity component normal to body axis

As a result of the normal velocity component $V \sin \alpha_B$ an additional velocity v_n is induced by the displacement of the normal flow about the body thusly:



so that the velocity vector diagram which includes this component is as follows:



where ϕ is the body-induced angle of attack and can be expressed as

$$\tan \phi = \frac{v_n \cos \alpha_B}{V + v_n \sin \alpha_B} \quad (A1)$$

For a circular cylinder, the total velocity parallel to the z axis at any point due to the normal flow is

$$V \sin \alpha_B + v_n = V \sin \alpha_B \left[\frac{R^2(y^2 - z^2)}{(y^2 + z^2)^2} + 1 \right] \quad (A2)$$

where R is the body radius. The incremental velocity v_n (from equation (A2)) becomes:

$$v_n = V \sin \alpha_B \left[\frac{R^2(y^2 - z^2)}{(y^2 + z^2)^2} \right] \quad (A3)$$

and the body-induced angle becomes by substitution of equation (A3) into equation (A1)

$$\phi = \tan^{-1} \left\{ \frac{V \sin \alpha_B \cos \alpha_B \left[\frac{R^2(y^2 - z^2)}{(y^2 + z^2)^2} \right]}{V + V \sin^2 \alpha_B \left[\frac{R^2(y^2 - z^2)}{(y^2 + z^2)^2} \right]} \right\} \quad (A4)$$

For small α_B

$$\cos \alpha_B \approx 1$$

$$\sin \alpha_B \approx \alpha_B$$

$$\tan \alpha_B \approx \alpha_B$$

and equation (A4) becomes

$$\phi = \frac{\alpha_B \left[\frac{R^2(y^2 - z^2)}{(y^2 + z^2)^2} \right]}{1 + \alpha_B^2 \left[\frac{R^2(y^2 - z^2)}{(y^2 + z^2)^2} \right]} \quad (A5)$$

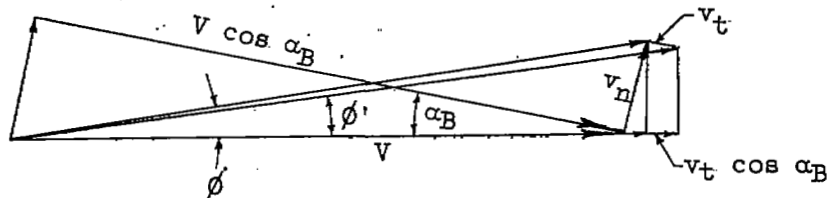
but

$$\alpha_B^2 \left[\frac{R^2(y^2 - z^2)}{(y^2 + z^2)^2} \right] \ll 1 \quad \text{for small } \alpha_B$$

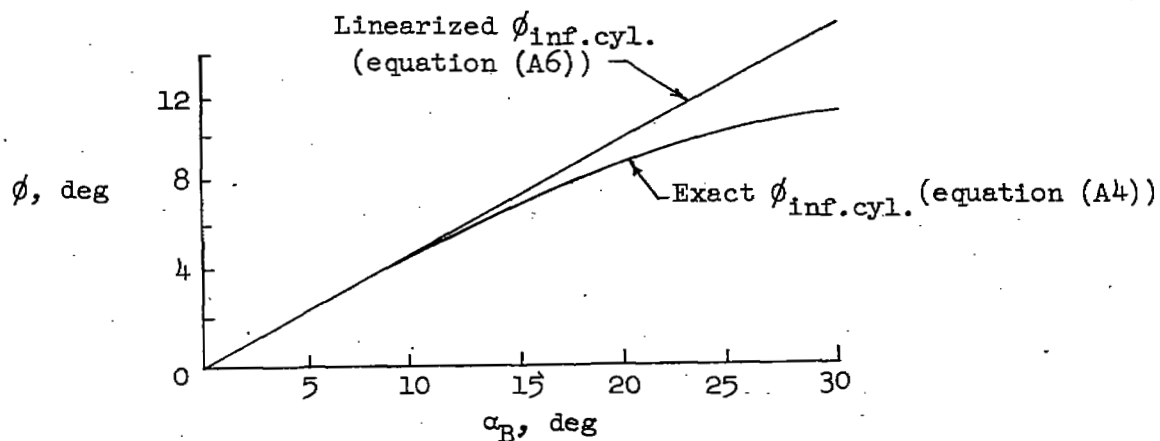
so that equation (A5) can be written:

$$\frac{\phi}{\alpha_B} \approx \left[\frac{R^2(y^2 - z^2)}{(y^2 + z^2)^2} \right] \quad (A6)$$

In assuming an infinite cylinder the tangential velocity increment v_t , due to the finite body length is neglected. The consequences of this are shown in the vector diagram below for the body used in these tests:



It can be seen that the tangential velocity increment v_t , reduces the body induced angle from ϕ to ϕ' and increases the free-stream velocity by $v_t \cos \alpha_B$. The body-induced lift then would be decreased by the former and increased by the latter (dynamic pressure increased) As a result of using the linearized equation (A6) in computing the body-induced angle of attack for the infinite cylinder, however, the amount of overprediction of the body-induced angle of attack nearly accounted for the velocity increment v_t at the higher angles of attack for these calculations. The amount of overprediction of the body-induced angle is shown below:



For example at $\alpha_B = 12.9^\circ$ and $\frac{2y}{b} = 0.10$, ϕ_{exact} (from equation A4) equals 5.83° whereas $\phi_{\text{linearized}}$ (from equation A6) equals 6.20° . The loading increment $\Delta c_l \frac{c}{c}$ due to the body would be approximately 0.016 smaller by using ϕ_{exact} instead of $\phi_{\text{linearized}}$. The correction to the dynamic pressure (due to $v_t \cos \alpha_B$) would increase the loading increment by 0.028. The net result of these two corrections would be 0.012 which for this extreme case was considered small enough to warrant the use of the linearized equation (A6) in computing the total body effect.

APPENDIX B

CALCULATION OF THE BODY EFFECTS USING THE 19×1 METHOD

The body-induced load distributions were calculated by using 19 horseshoe vortices distributed along the $0.25c$ line at $\frac{zy}{b} = 0, \pm 0.10, \pm 0.20, \dots, \pm 0.90$. The downwash induced by these vortices at the $0.75c$ line of the wing at these same spanwise stations was set equal to the angle of attack of the wing at the $0.75c$ line. Since the loading was symmetrical, the loading at the corresponding points in each semi-span were identical so that 10 equations in the 10 unknown loadings $\left(\frac{c_l c}{c}\right)_n$ resulted as follows:

$$(\alpha_{0.75c})_n = \sum_{n=1}^{n=10} K_n \left(\frac{c_l c}{c}\right)_n \quad (B1)$$

where

n spanwise station, ($n = 1$ at $\frac{zy}{b} = -0.90$ and $n = 10$ at $\frac{zy}{b} = 0$.)

K_n downwash factor at $0.75c$ line.

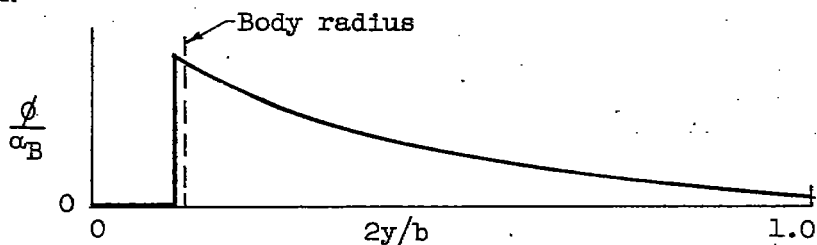
This method can be considered as a modified Falkner method for calculating the wing spanwise loading and follows a procedure similar to those indicated in references 21 and 22.

The body effect was treated as a twist distribution so that the angle of attack at the $0.75c$ line at each station was set equal to the body-induced angle of attack

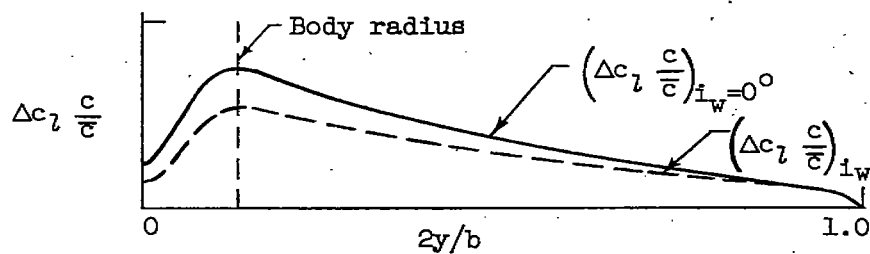
$$(\alpha_{0.75c})_n = \alpha_B \left(\frac{\phi}{\alpha_B}\right)_n \quad (B2)$$

where $\alpha_B = \alpha - i_w$ and $\left(\frac{\phi}{\alpha_B}\right)_n$ was obtained by using equation (A6) for $z = 0.5R$ (mid-high-wing position) at spanwise stations corresponding to those of the lifting elements. The body-induced angle was assumed to

be zero at the plane of symmetry resulting in the following angle distribution:



Simultaneous solutions of the systems of equations (B1) gave the following load distributions:



The loadings at any other angles of attack or angles of incidence were obtained by direct proportion since the linearized $\frac{\phi}{\alpha_B}$ variation was used.

REFERENCES

1. Möller, E.: Systematische Druckverteilungsmessungen an Flügel/Rumpf - Anordnungen. (Tief-, Mittel-, Schulter-, und Hochdecker). Bericht 44/22, Aerodynamisches Institut der T. H. Braunschweig, Dec. 27, 1944.
2. Tunnel Staff of Aero. Dept.: Low Speed Pressure Distributions on a 59° Swept Wing and Comparison with High Speed Results on a 45° Swept Wing. Rep. No. Aero. 2311, British R.A.E., Feb. 1949.
3. Jacobs, Willi: Lift and Moment Changes Due to the Fuselage for a Yawed Aeroplane with Unswept and Swept Wings. Rep. No. 34, Aero. Res. Inst. of Sweden, (Stockholm) 1950.
4. Holme, O.: Comparative Wind Tunnel Tests of a Swept-Back and a Straight Wing Having Equal Aspect Ratios. Rep. No. 31, Aero. Res. Inst. of Sweden (Stockholm), 1950.
5. Lennertz, J.: Influence of the Airplane Body on the Wings. Vol. IV of Aerodynamic Theory, div. K, ch. III, sec. 1, W. F. Durand, ed., Julius Springer (Berlin), 1935, pp. 152-157.
6. Vladea, Joan: Effect of Fuselage and Engine Nacelles on Some Aerodynamic Properties of an Airplane Wing. NACA TM 736, 1934.
7. Vandrey, Von F.: Zur theoretischen Behandlung des gegenseitigen Einflusses von Tragflügel und Rumpf. Luftfahrtforschung, Bd. 14, Lfg. 7, Sept. 7, 1937, pp. 347-355.
8. Multhopp, H.: Aerodynamics of the Fuselage. NACA TM 1036, 1942.
9. Pepper, Perry A.: Minimum Induced Drag in Wing-Fuselage Interference. NACA TN 812, 1941.
10. Spreiter, John R.: Aerodynamic Properties of Slender Wing-Body Combinations at Subsonic, Transonic, and Supersonic Speeds. NACA TN 1662, 1948.
11. Zlotnick, Martin, and Diederich, Franklin W.: Theoretical Calculation of the Effect of the Fuselage on the Spanwise Lift Distribution on the Wing. NACA RM L51J19, 1951.
12. Hopkins, Edward J., and Carel, Hubert C.: Experimental and Theoretical Study of the Effects of Body Size on the Aerodynamic Characteristics of an Aspect-Ratio 3.0 Wing-Body Combination. NACA RM A51G24, 1951.

13. Graham, Robert R.: Low-Speed Characteristics of a 45° Sweptback Wing of Aspect Ratio 8 from Pressure Distributions and Force Tests at Reynolds Numbers from 1,500,000 to 4,800,000. NACA RM L51H13, 1951.
14. Schneider, William C.: A Comparison of the Spanwise Loading Calculated by Various Methods with Experimental Loadings Obtained on a 45° Sweptback Wing of Aspect Ratio 8 at a Reynolds Number of 4.0×10^6 . NACA RM L51G30, 1952.
15. Pratt, George L., and Shields, E. Rousseau: Low-Speed Longitudinal Characteristics of a 45° Sweptback Wing of Aspect Ratio 8 with High-Lift and Stall-Control Devices at Reynolds Numbers from 1,500,000 to 4,800,000. NACA RM L51J04, 1951.
16. Salmi, Reino J., and Jacques, William A.: Effect of Vertical Location of a Horizontal Tail on the Static Longitudinal Stability Characteristics of a 45° Sweptback-Wing - Fuselage Combination of Aspect Ratio 8 at a Reynolds Number of 4.0×10^6 . NACA RM L51J08, 1951.
17. Sivells, James C., and Salmi, Rachel M.: Jet-Boundary Corrections for Complete and Semispan Swept Wings in Closed Circular Wind Tunnels. NACA TN 2454, 1951.
18. Zahm, A. F.: Flow and Drag Formulas for Simple Quadrics. NACA Rep. 253, 1927.
19. Neumark, S.: Velocity Distribution on Thin Bodies of Revolution at Zero Incidence in Incompressible Flow. Rep. No. Aero 2389, British R.A.E., July 1950.
20. Hartley, D. E.: Low Speed Wind Tunnel Tests on Asymmetrically Situated Circular Cylindrical Bodies on a Straight and a 45° Sweptback Wing. Rep. No. Aero 2349, British R.A.E., Dec. 1949.
21. Diederich, Franklin W.: Charts and Tables for Use in Calculations of Downwash of Wings of Arbitrary Plan Form. NACA TN 2353, 1951.
22. Campbell, George S.: A Finite-Step Method for the Calculation of Span Loadings of Unusual Plan Forms. NACA RM L50L13, 1951.

TABLE I.- ORDINATES FOR CAMBER LINE OF TWISTED AND CAMBERED WING

[All values are given in percent of chord.]

x/c	z/c ^a	x/c	z/c ^a
0	0	40	5.310
.5	.262	45	5.407
.75	.369	50	5.428
1.25	.566	55	5.372
2.5	.991	60	5.240
5.0	1.689	65	5.028
7.5	2.256	70	4.733
10	2.731	75	4.350
15	3.496	80	3.861
20	4.070	85	3.257
25	4.525	90	2.490
30	4.874	95	1.522
35	5.132	100	0



$${}^a \left[\frac{z}{c} \right]_{c_l=1.0} = \frac{1}{1.05} \left[\left(\frac{z}{c} \right)_{a=1.0} + \frac{1}{6} \left(\frac{z}{c} \right)_{230} \right]$$

TABLE II.- CHORDWISE ORIFICE LOCATIONS

[Locations given in percent of chord from leading edge]

Plane wing, twisted and cambered wing		Plane wing	Twisted and cambered wing	
All stations except 0.03b/2		0.03b/2	0.03b/2	
Upper surface	Lower surface	Upper and lower surface	Upper surface	Lower surface
0	-----	0	0	-----
.10	-----	-----	-----	-----
.25	-----	-----	-----	-----
.50	-----	-----	-----	-----
1.25	1.25	1.25	1.25	1.25
2.50	-----	-----	2.50	-----
-----	3.75	-----	-----	3.75
5.00	-----	5.00	5.00	-----
-----	7.50	-----	-----	7.50
8.50	-----	8.50	8.50	-----
15.00	15.00	15.00	15.00	15.00
25.00	25.00	25.00 ^a	25.00	(c)
35.00	35.00	(b)	-----	-----
45.00	45.00	-----	45.00	-----
55.00	55.00	-----	-----	-----
65.00	65.00	-----	65.00	-----
75.00	75.00	-----	-----	-----
85.00	85.00	-----	-----	-----
95.00	95.00	-----	95.00	95.00

^aUpper surface only.^bMeasurements rearward of 0.25c made at 0.10c intervals with static pressure survey tube.^cMeasurements rearward of 0.15c made at 0.10c intervals with static pressure survey tube.

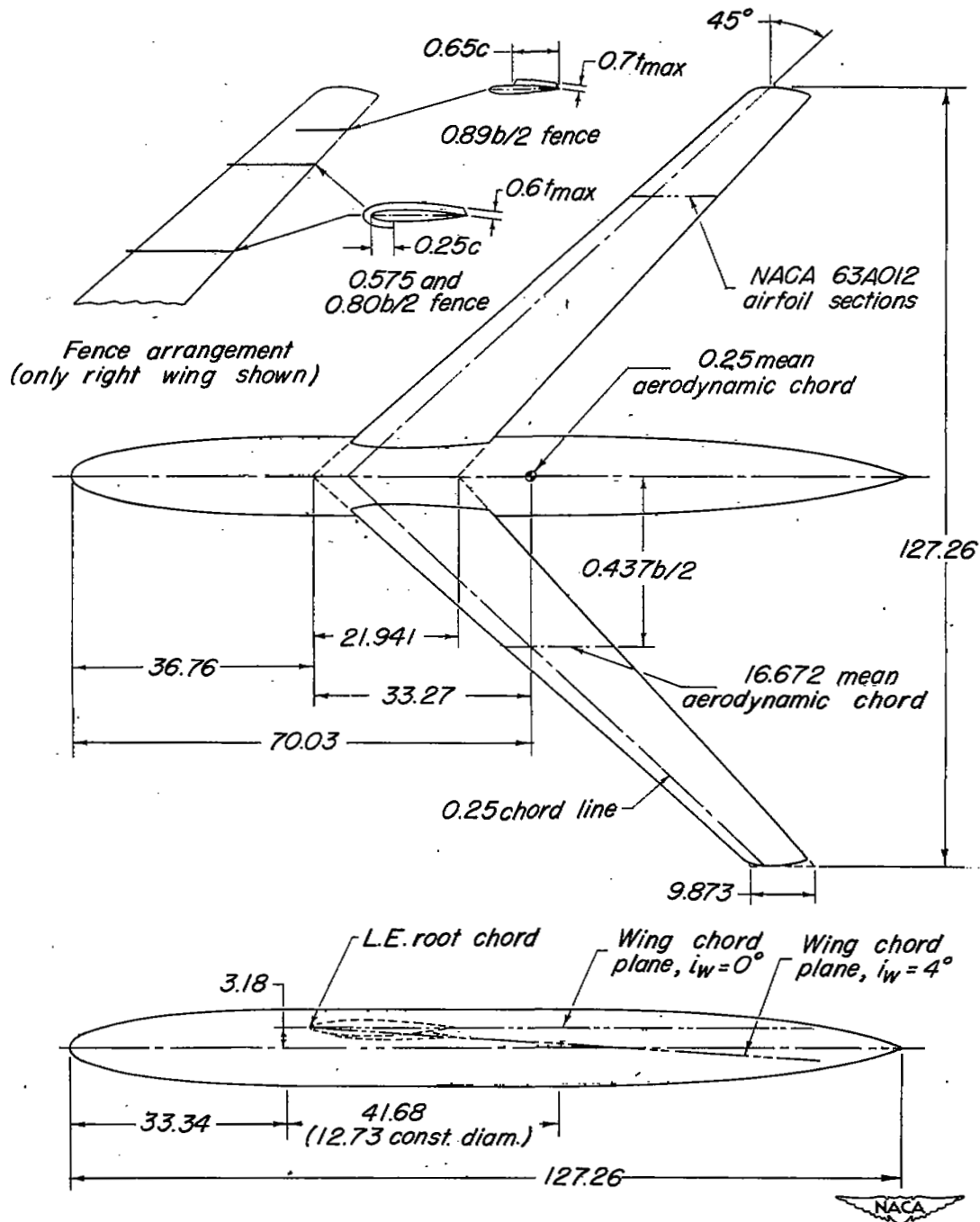
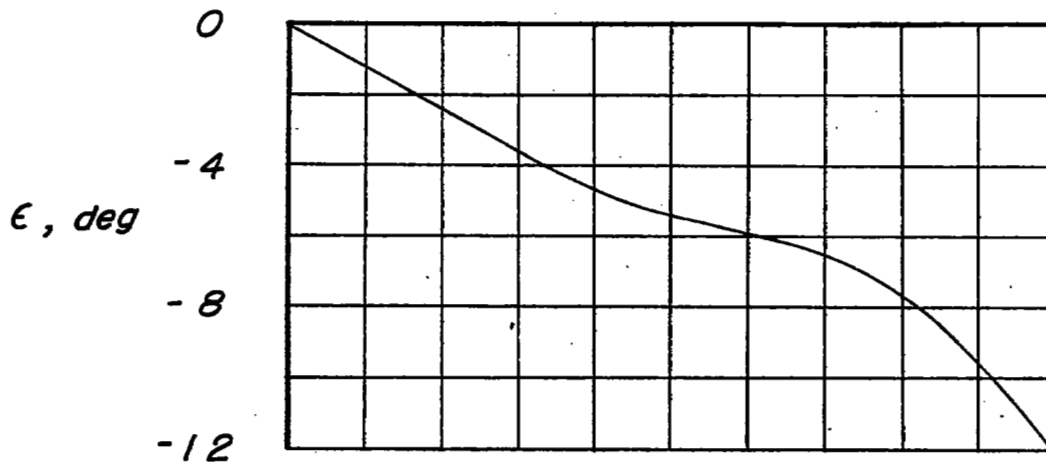
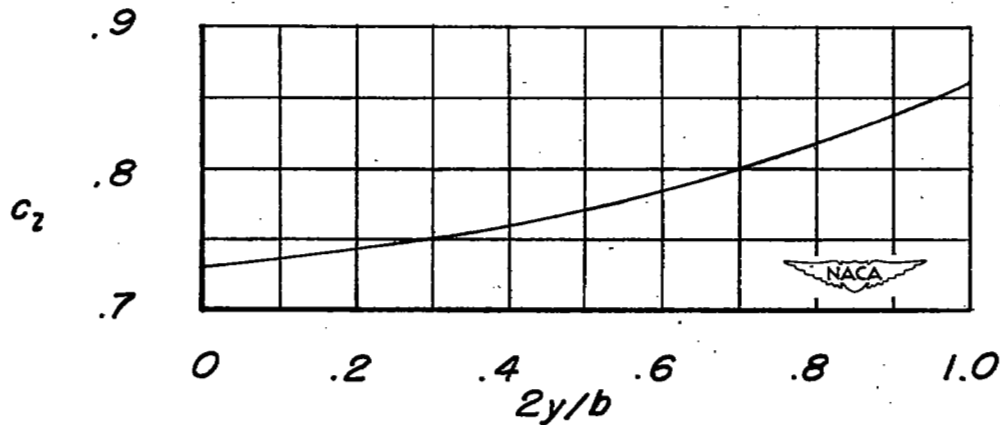


Figure 1.- Geometric details of the plane wing-body combination and fence arrangement. Wing taper ratio 0.45; aspect ratio 8.02; wing area 14.021 ft.²; no twist. All dimensions are in inches unless noted.



(a) Design twist distribution.



(b) Design lift coefficient.

Figure 2.- Design characteristics of the twisted and cambered wing.
 NACA 63₁A012 thickness distribution used throughout.

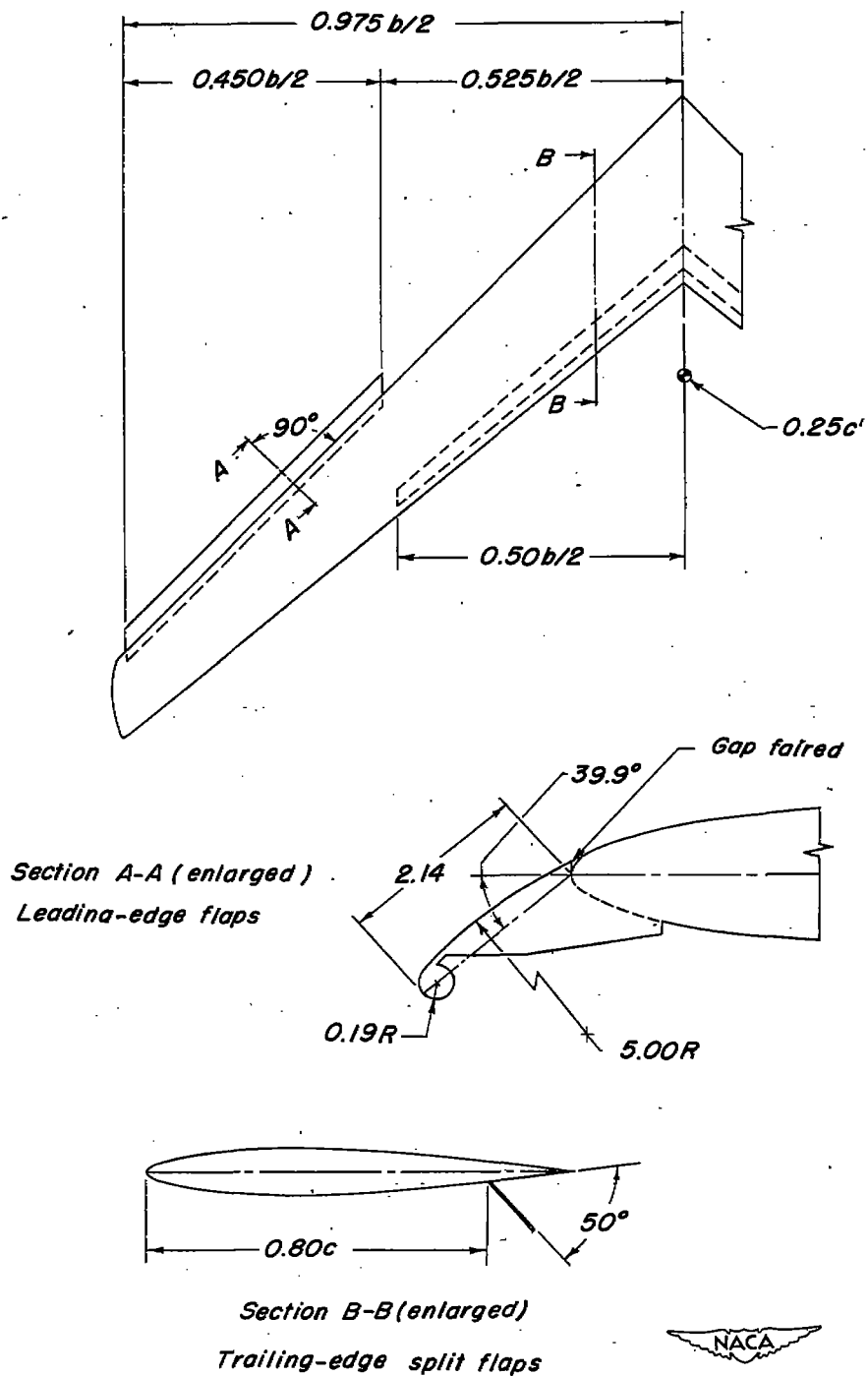


Figure 3.- Details of flap configuration. All dimensions are in inches unless noted.

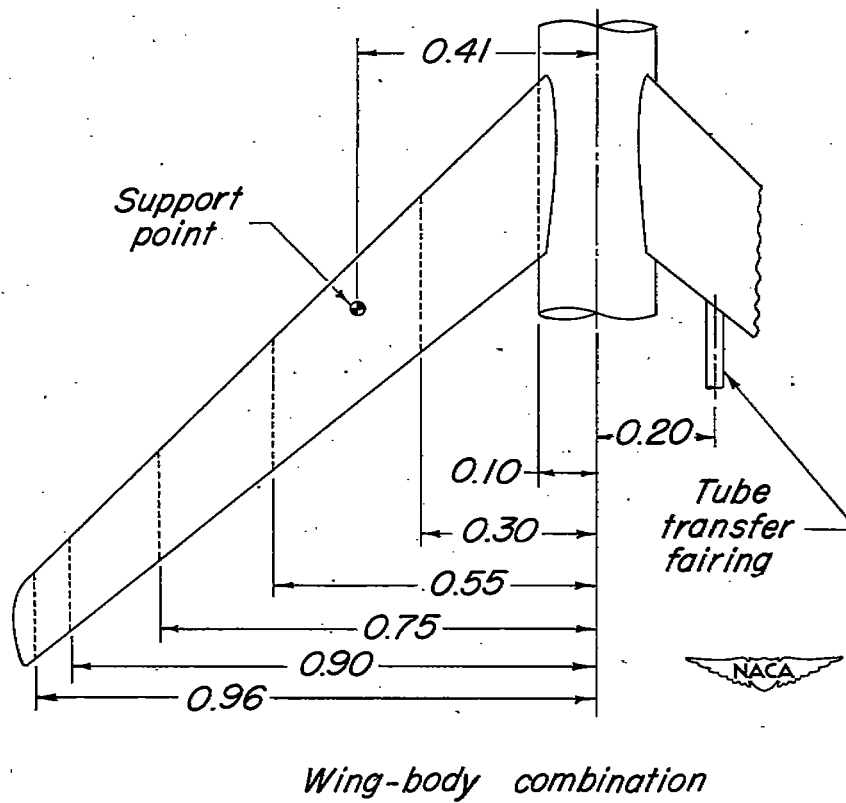
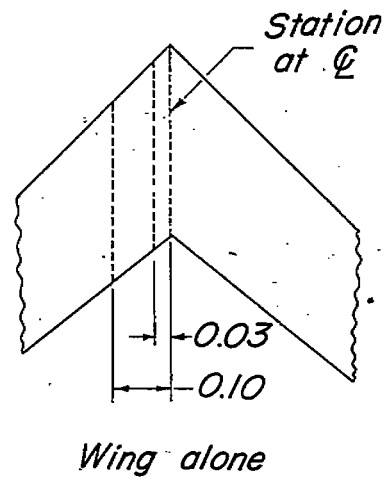


Figure 4.- Spanwise locations of orifice stations on left wing. All dimensions are in fraction of semispan.

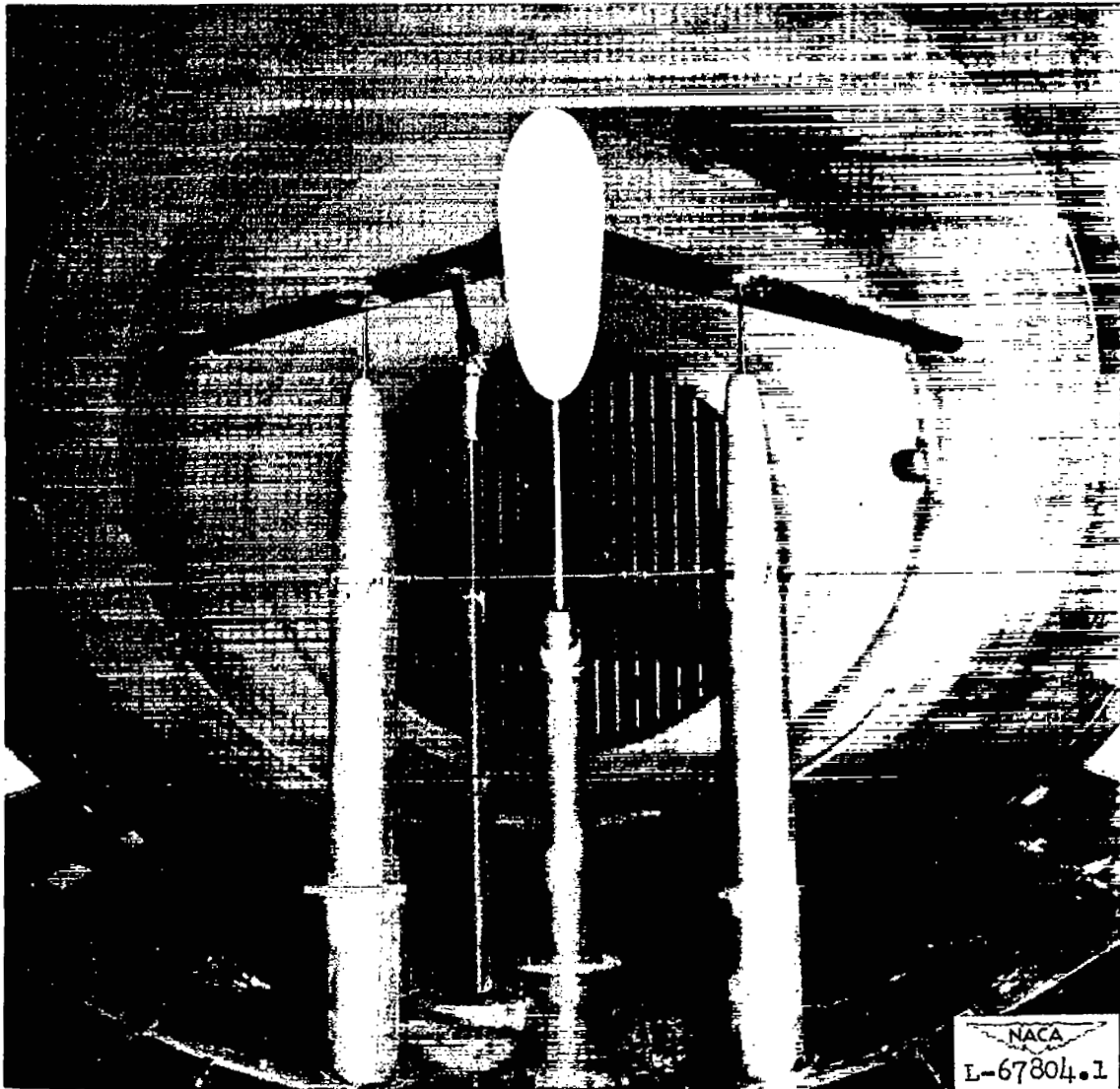
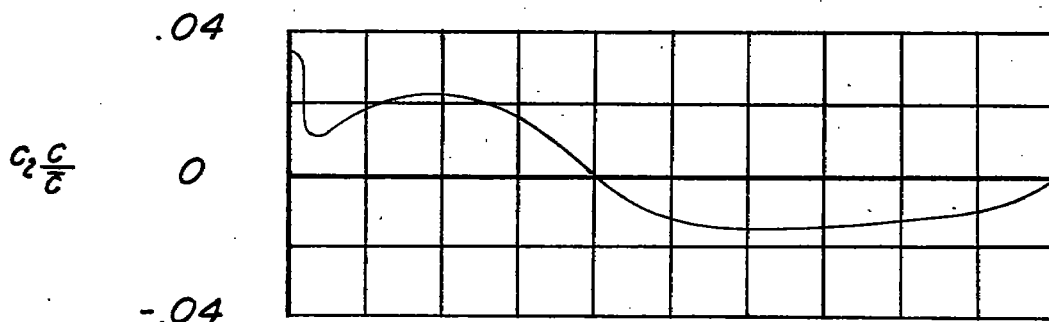
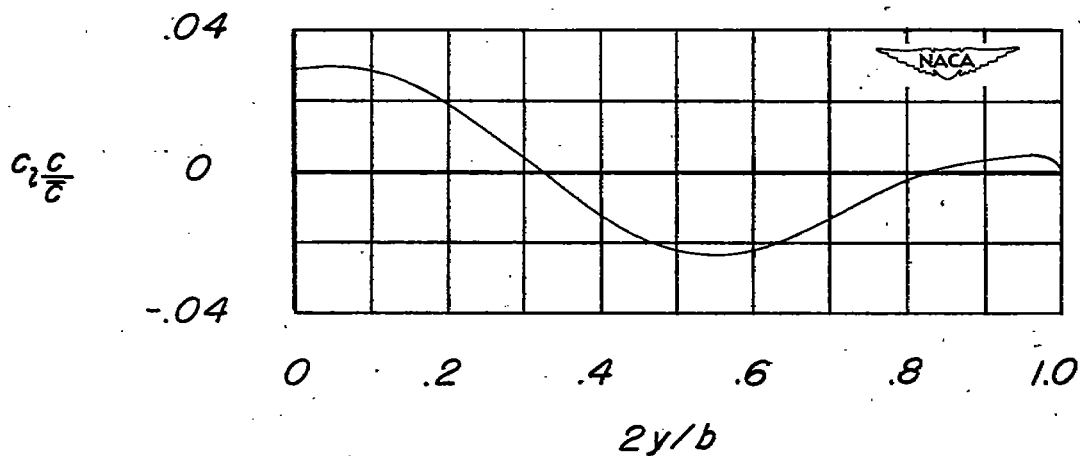


Figure 5.- Wing-body combination as mounted in the Langley 19-foot pressure tunnel for pressure distribution tests.



(a) Plane wing.



(b) Twisted and cambered wing.

Figure 6.- Corrections to the experimental load distributions due to air stream misalignment.

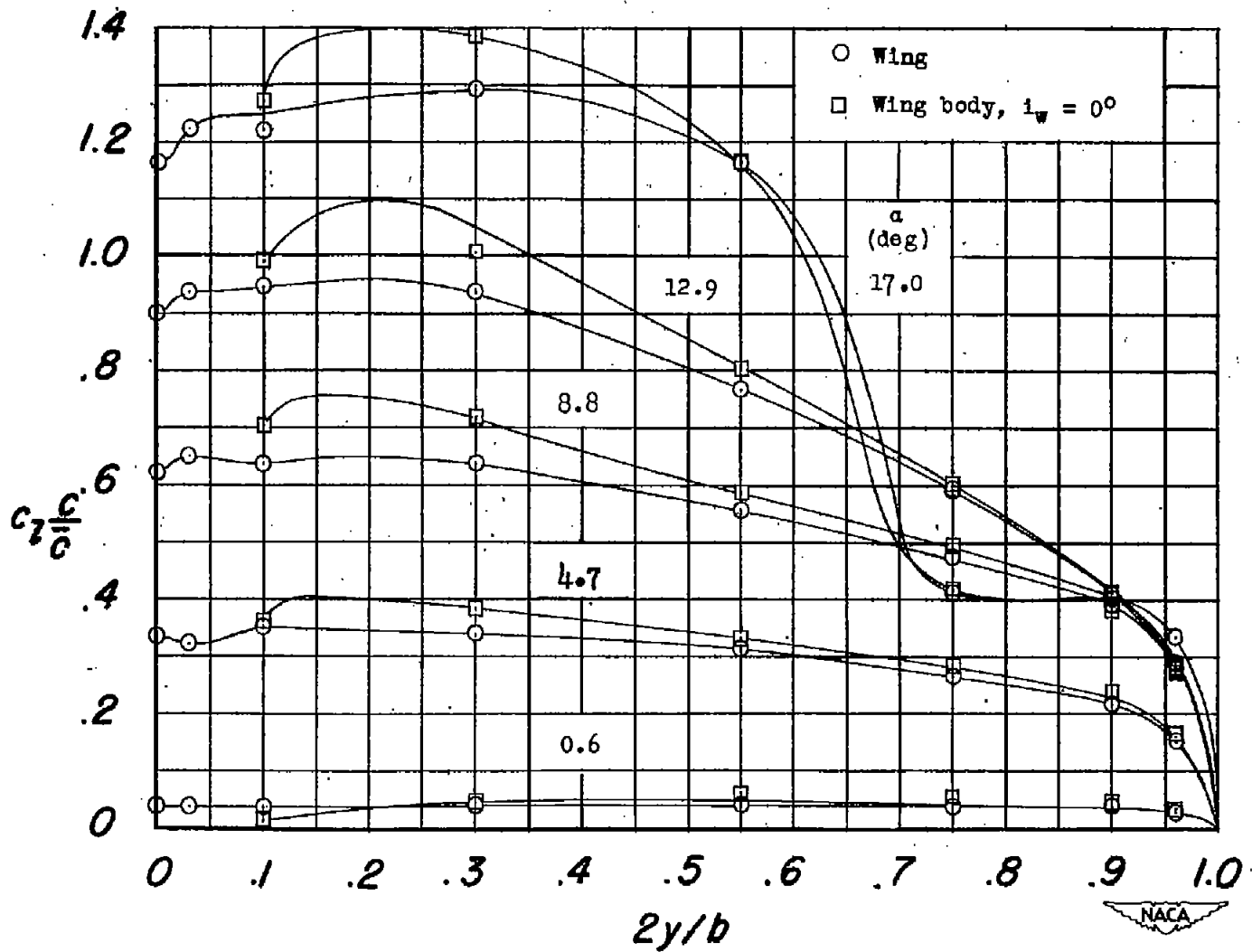


Figure 7.- Effects of body on the plane wing spanwise load distributions.

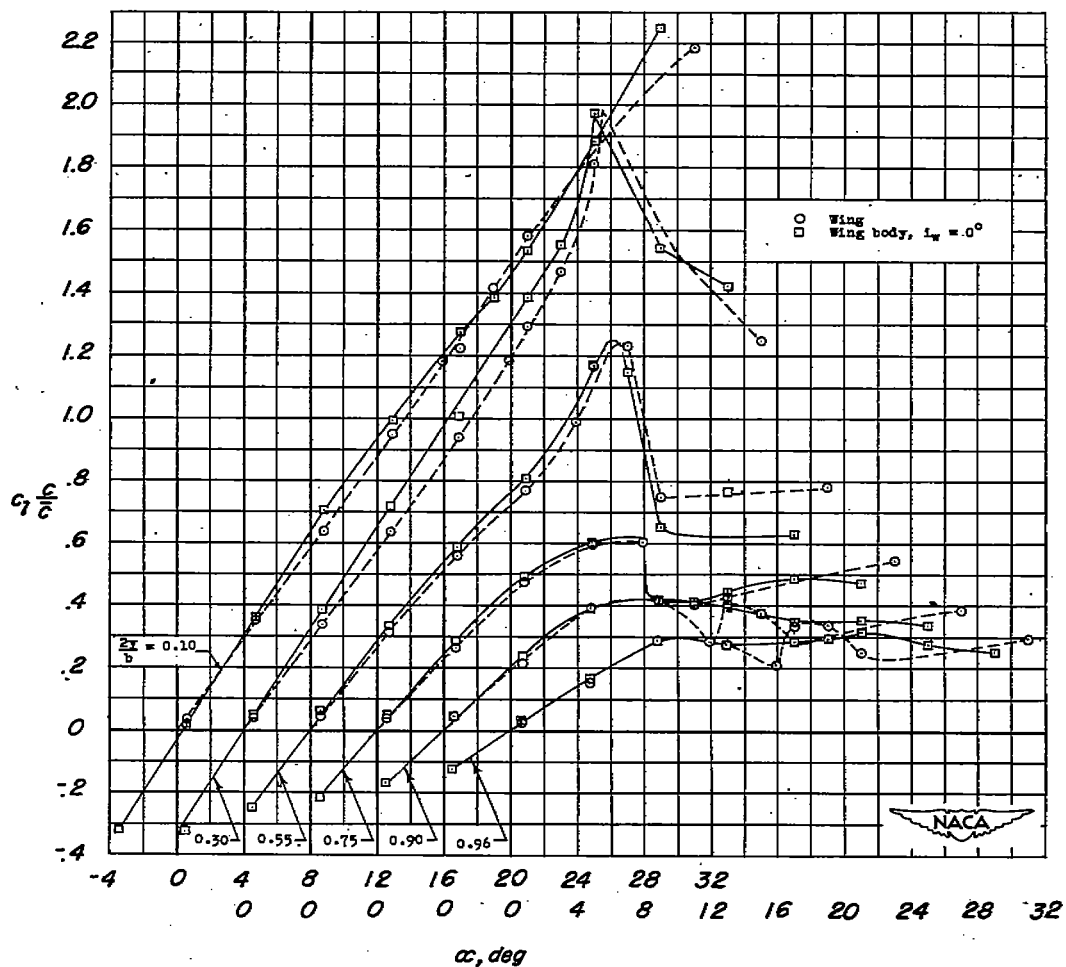


Figure 8.- Effects of body on the variation of the section load coefficients with angle of attack for the plane wing, $i_w = 0^\circ$.

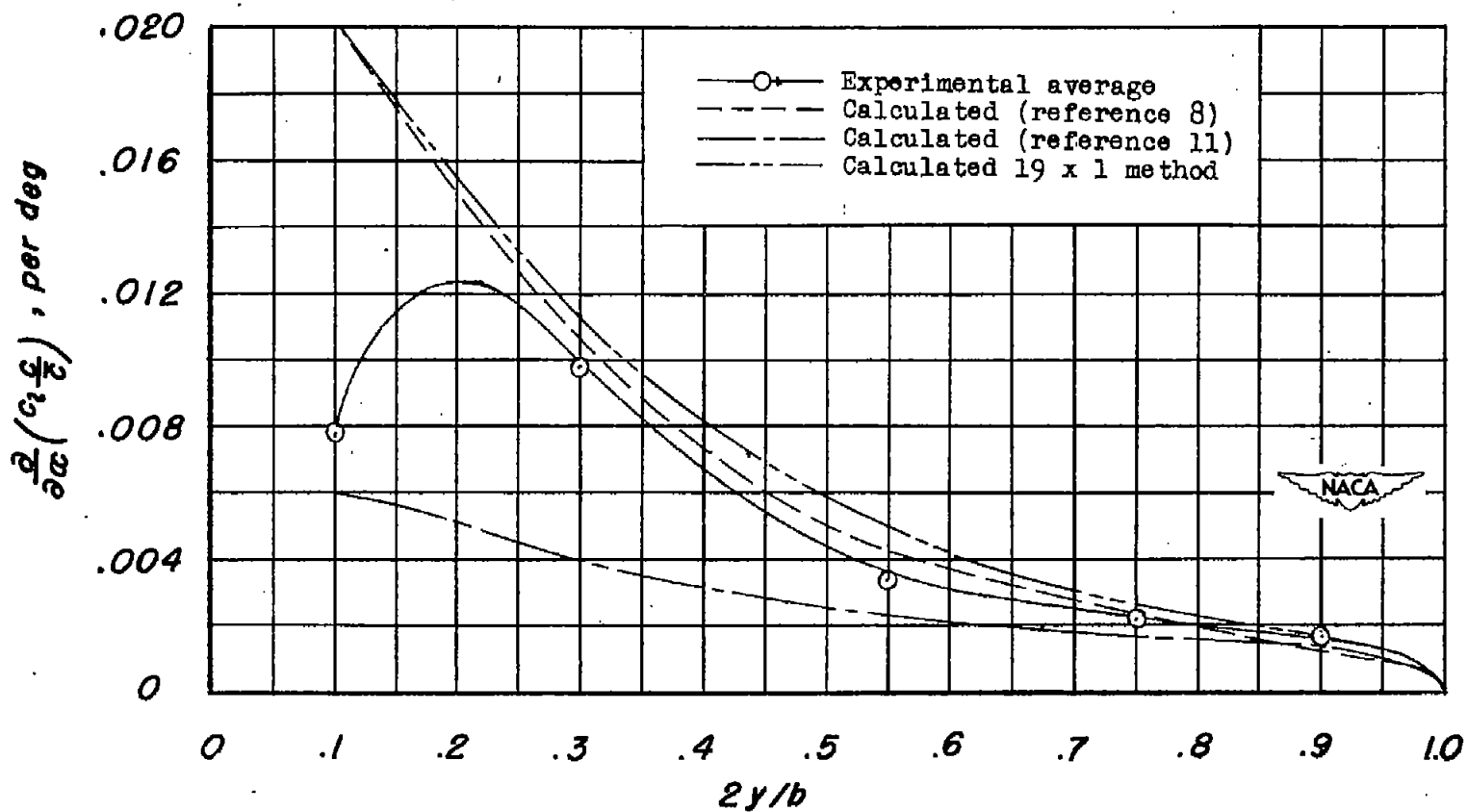


Figure 9.- Comparisons between the calculated and experimental variations with angle of attack of the span load distribution induced by the body on the plane wing.

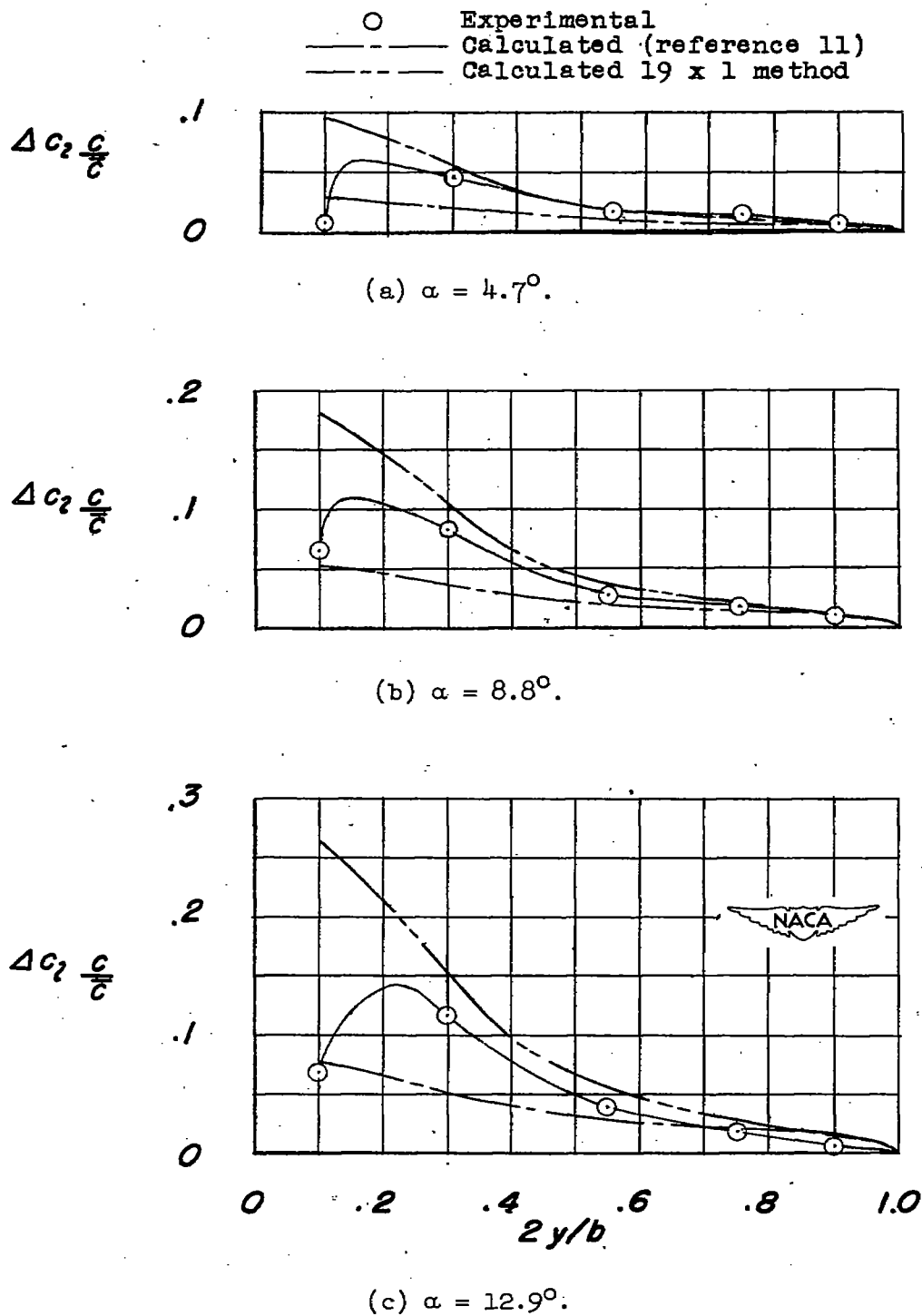
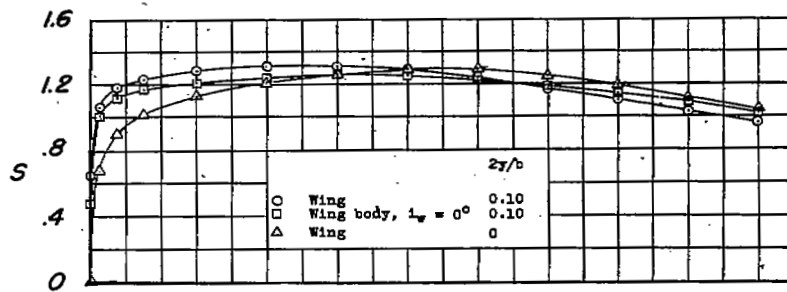
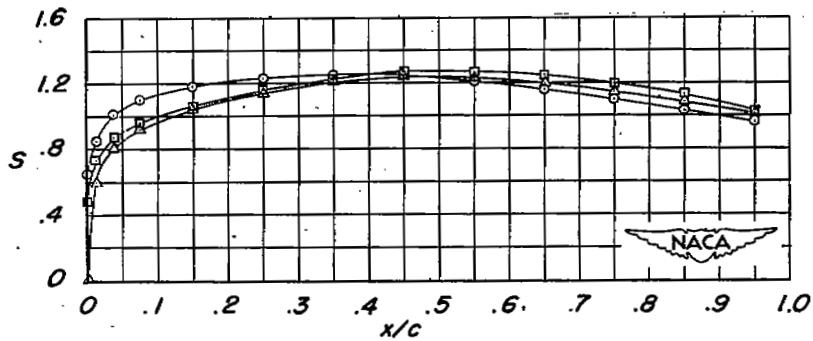


Figure 10.- Incremental load distributions due to the addition of the body on the plane wing and comparison with calculated distributions, $i_w = 0^\circ$.



(a) Upper surface.



(b) Lower surface.

Figure 11.- Comparisons between the pressure distributions at $0.10b/2$ with and without body and at the plane of symmetry of the plane wing. $\alpha = 0.6^\circ$.

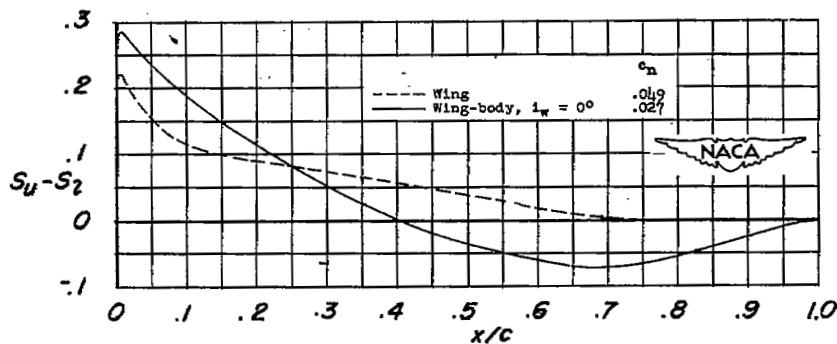


Figure 12.- Chordwise load distributions at $0.10b/2$ with and without body. $\alpha = 0.6^\circ$.

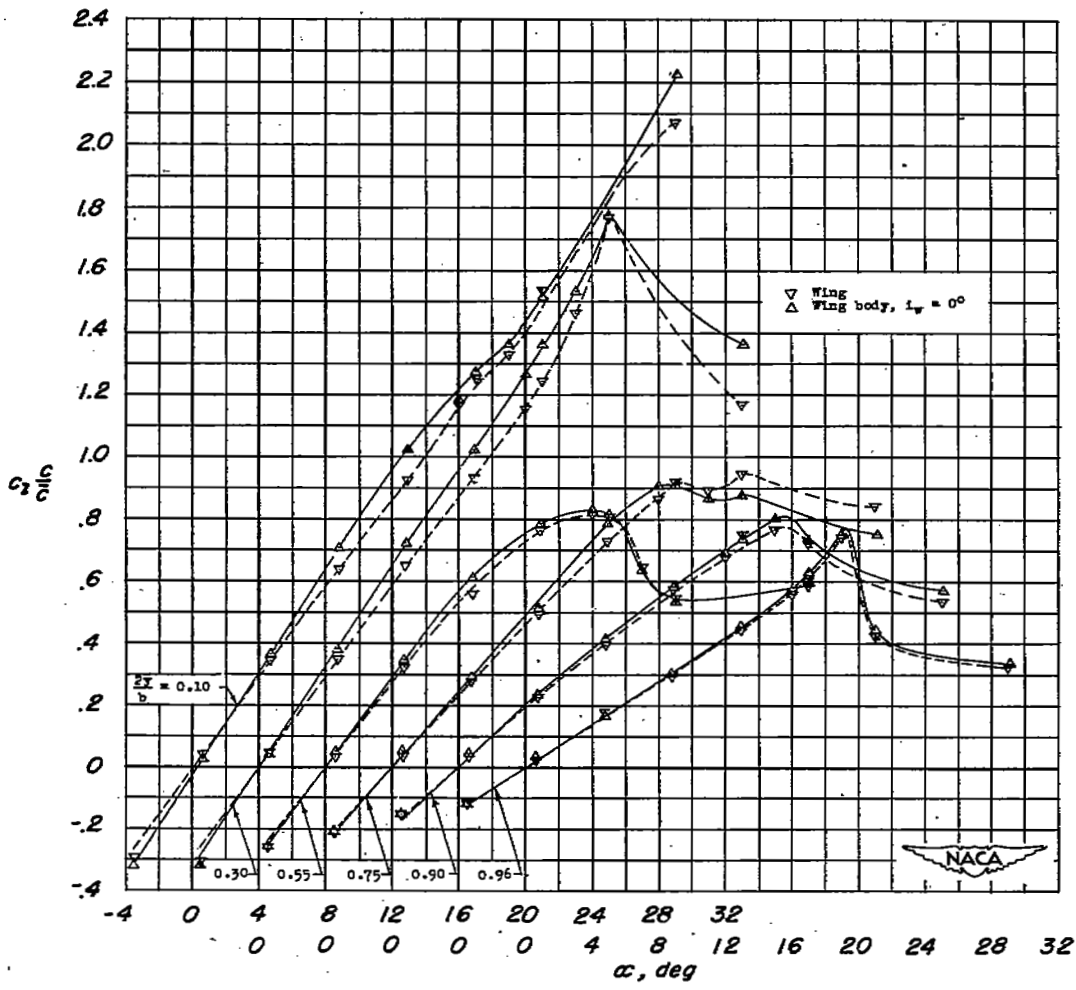


Figure 13.- Effects of body on the variation of the section load coefficients with angle of attack for the plane wing with upper-surface fences at $0.575b/2$, $0.80b/2$, and $0.89b/2$.

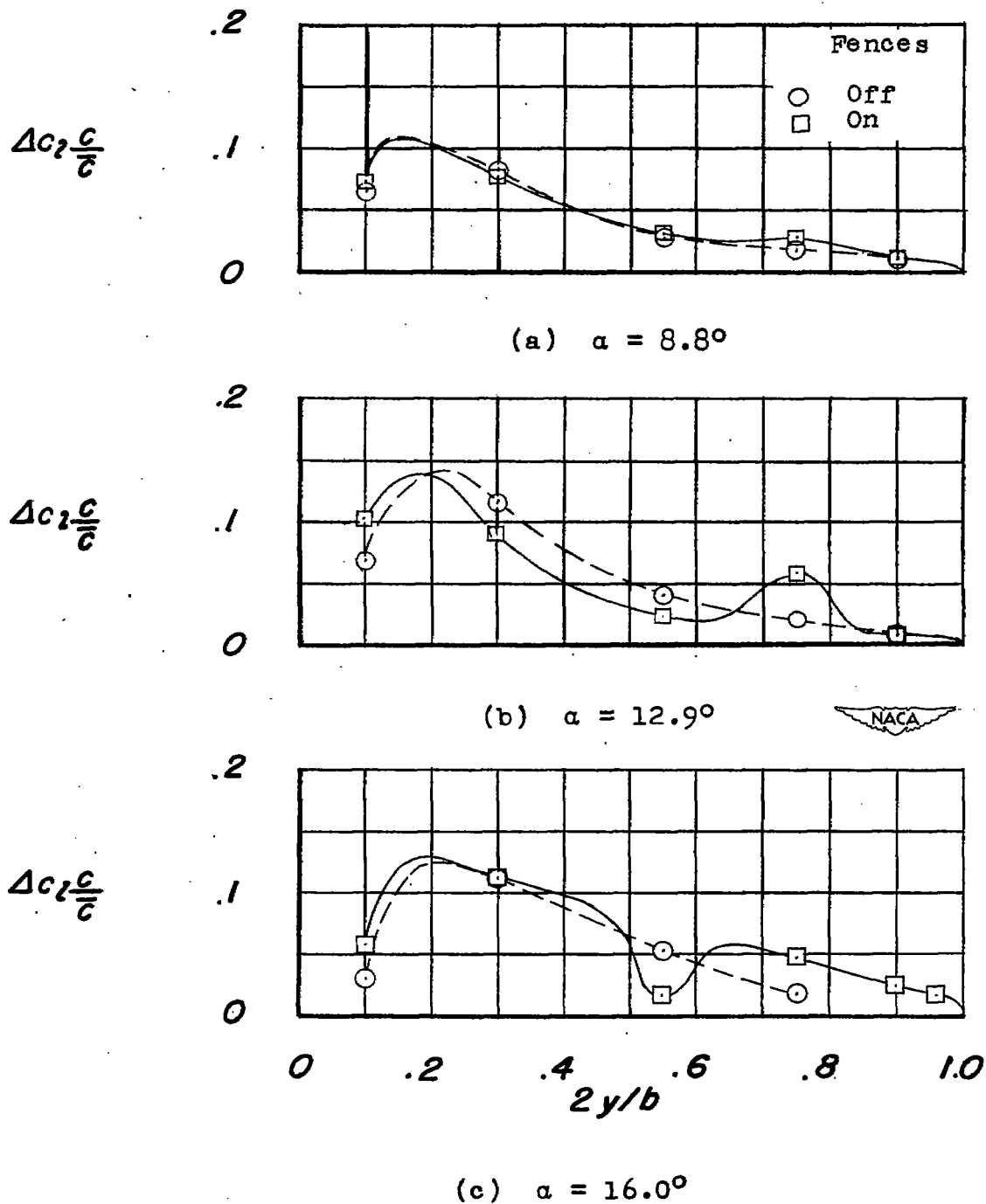


Figure 14.- Effects of upper-surface fences on the incremental load distribution due to the addition of the body on the plane wing. $i_w = 0^\circ$. Upper-surface fences located at $0.575b/2$, $0.80b/2$, and $0.89b/2$.

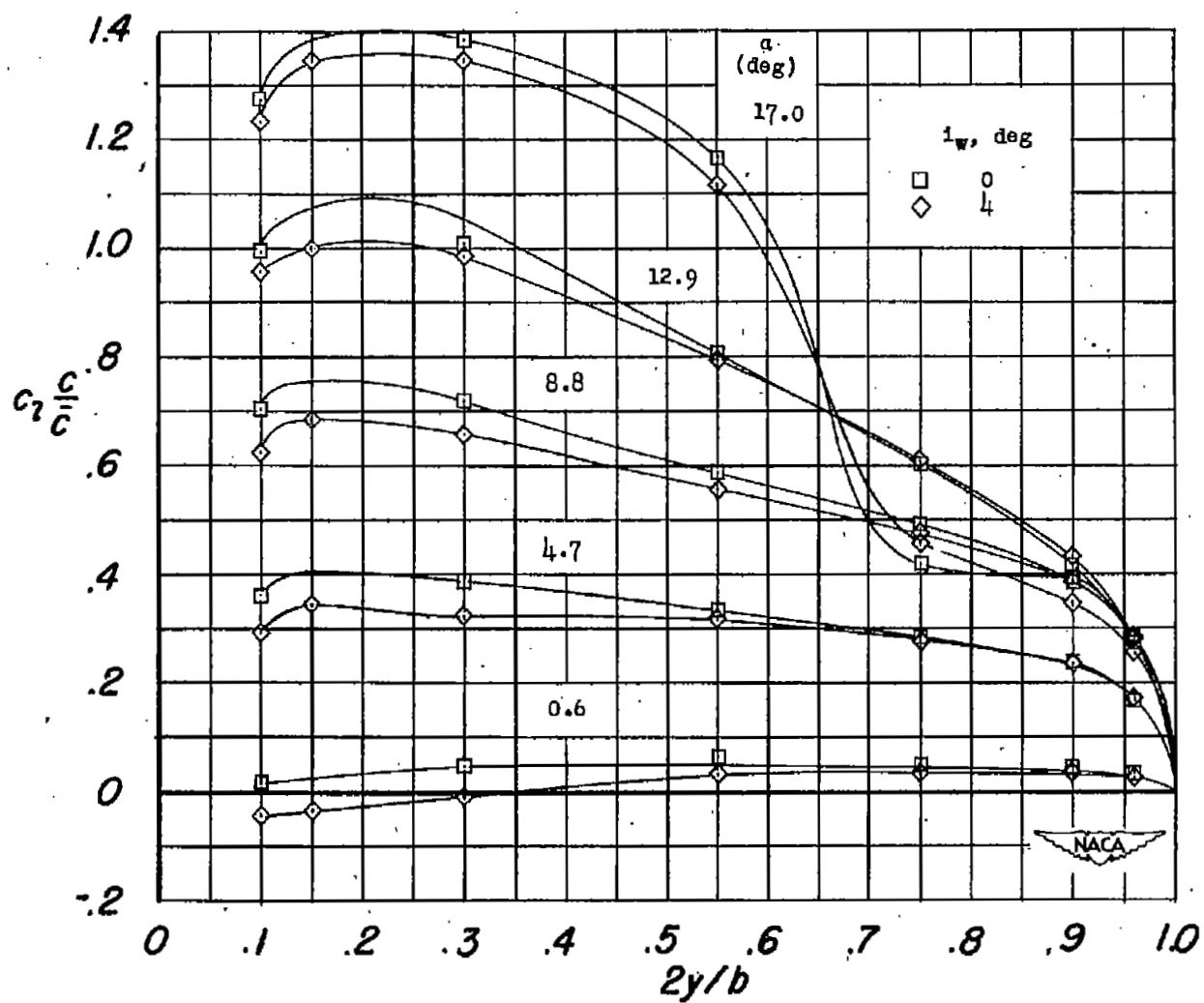


Figure 15.- Effects of changing the wing incidence on the spanwise load distribution over the plane wing-body combination.

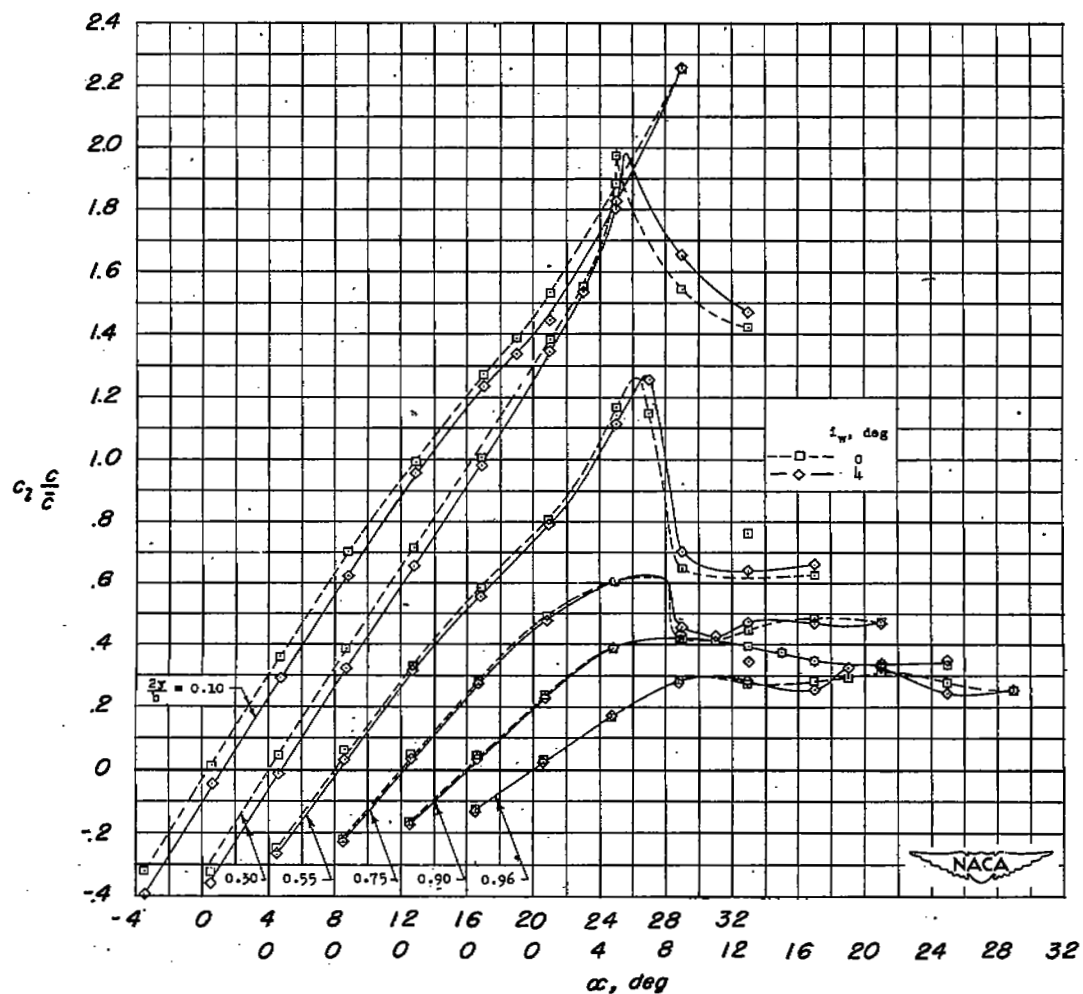
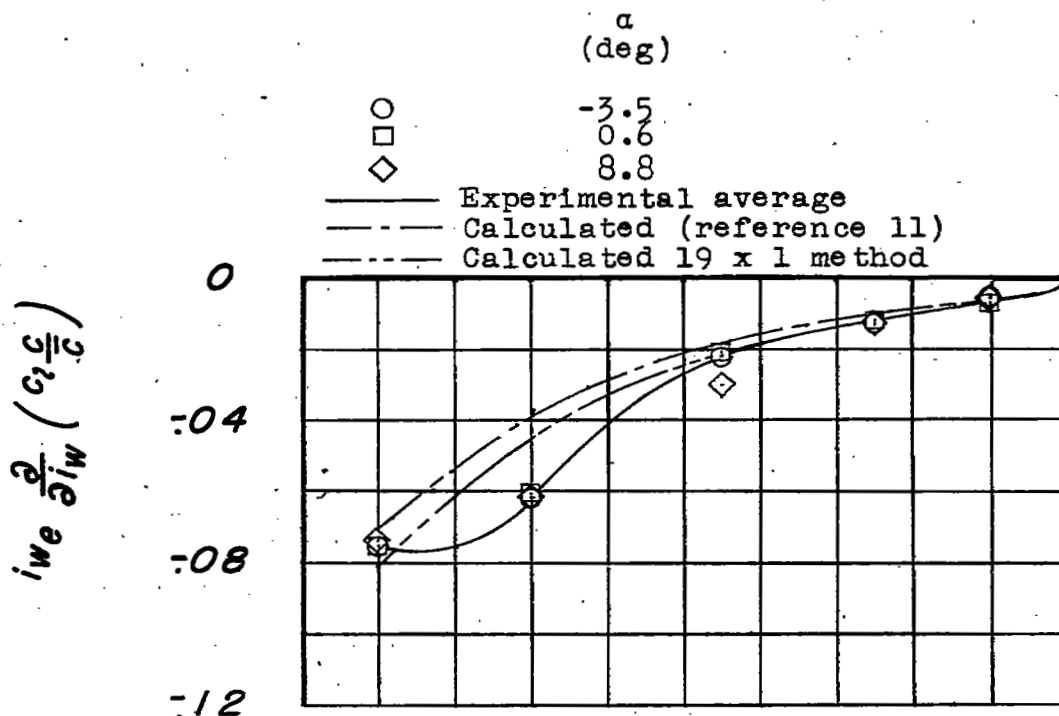
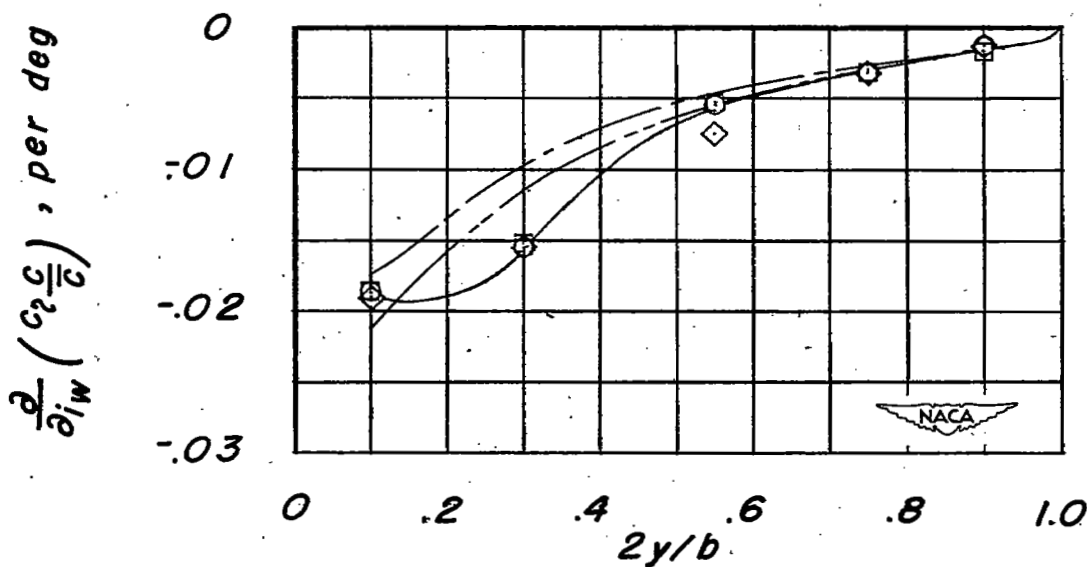


Figure 16.- Effects of changing the wing incidence on the variation of section load coefficients with angle of attack of the plane wing-body combination.

(a) Incremental loading for 4° change of wing incidence.

(b) Incremental loading per unit change of wing incidence.

Figure 17.- The spanwise variations of the incremental load distributions due to changing the wing incidence with respect to the body for the plane wing and comparison with the calculated variations.

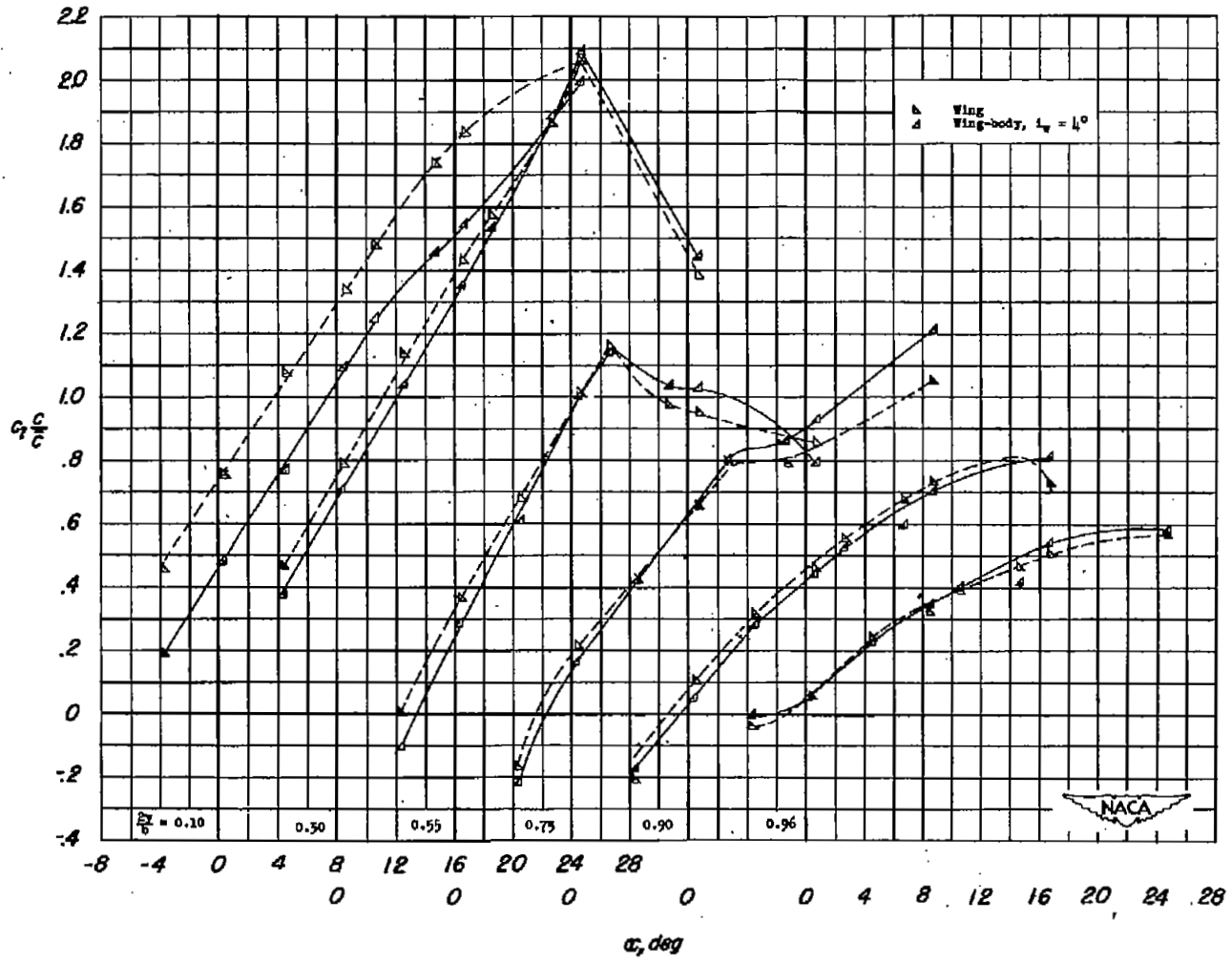


Figure 18.- Effects of body on the variations of the section load coefficients with angle of attack for the plane wing. 0.45b/2 leading-edge flaps and 0.50b/2 trailing-edge split flaps deflected 50°.

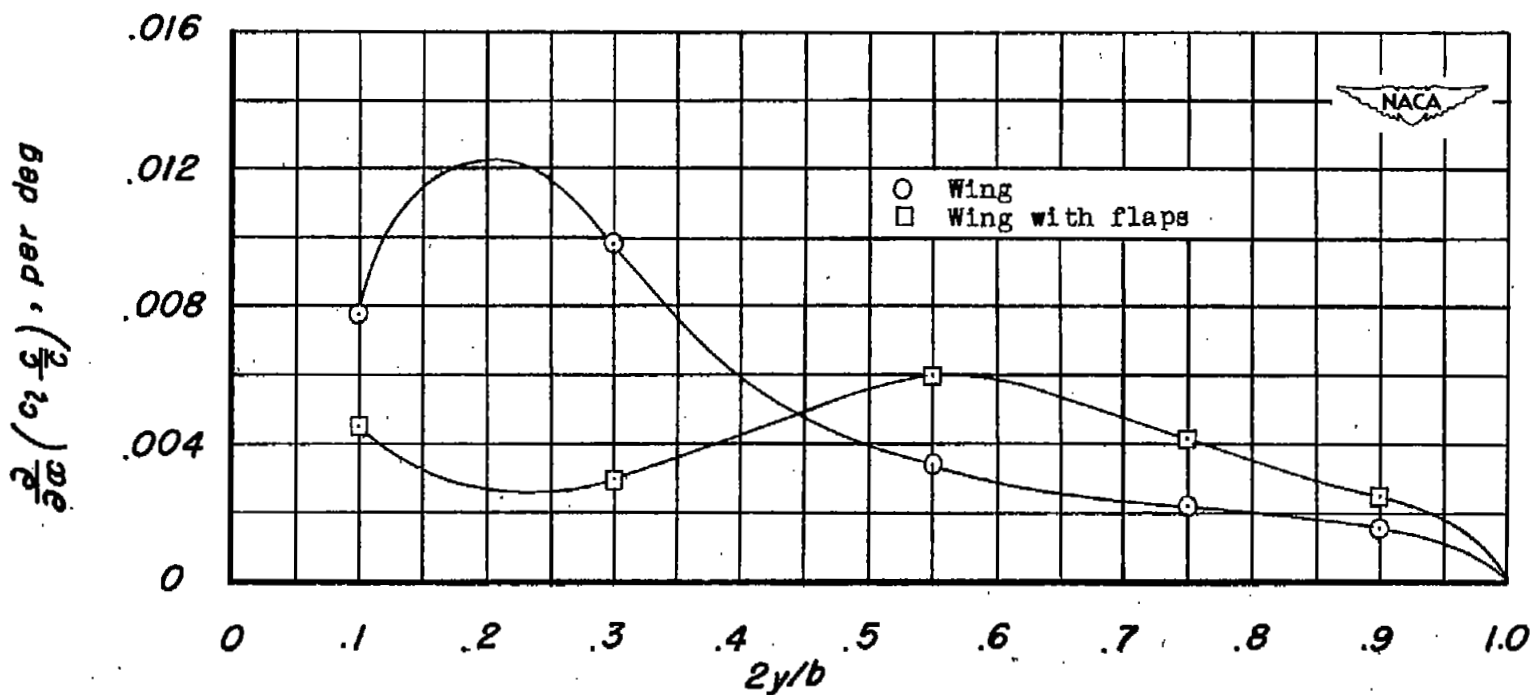


Figure 19.- Effects of deflecting $0.45b/2$ leading-edge flaps and 0.50 trailing-edge split flaps on the variations with angle of attack of the incremental loadings due to the addition of the body on the plane wing.

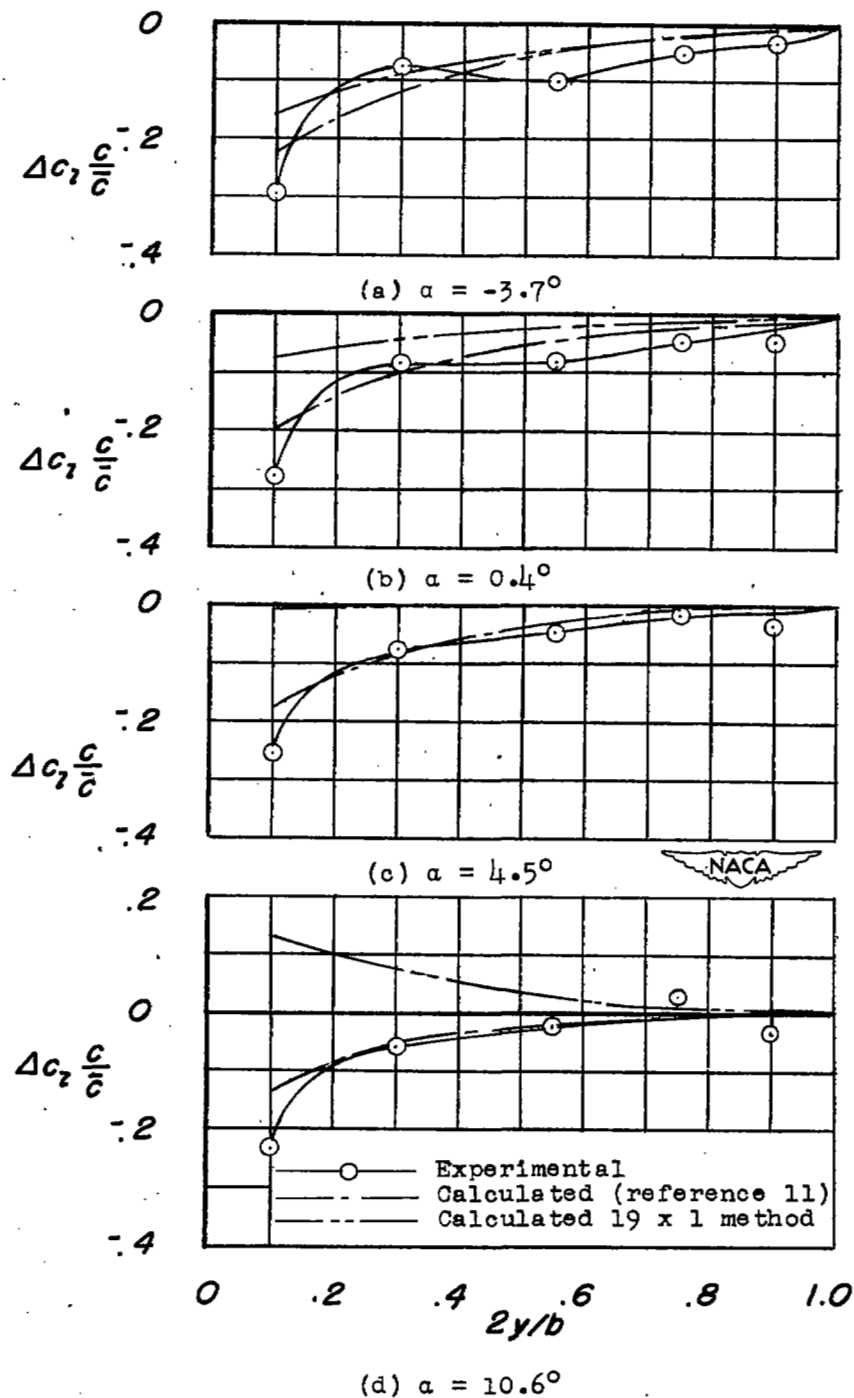


Figure 20.- Experimental and calculated incremental load distributions due to the addition of body on the plane wing. $0.45b/2$ leading-edge flaps and $0.50b/2$ trailing-edge split flaps deflected 50° . $i_w = 4^\circ$.

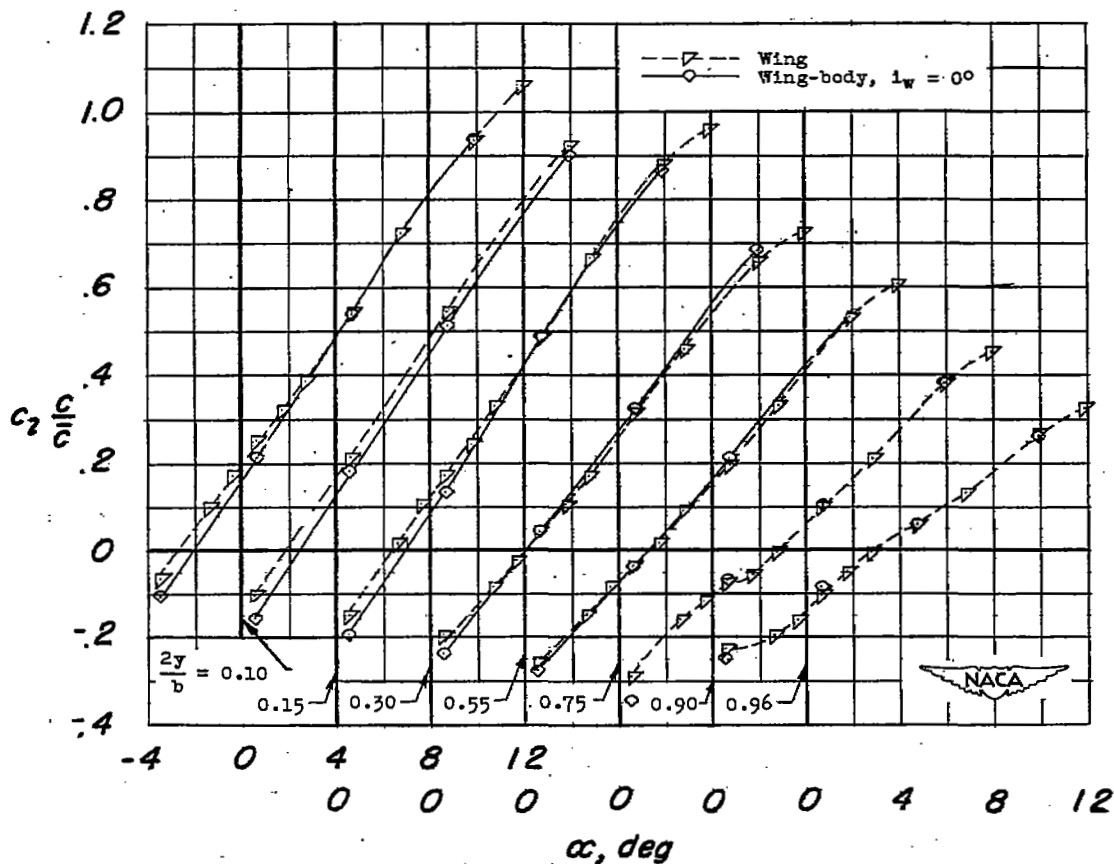


Figure 21.- Effects of body on the variations of the section load coefficients with angle of attack for the twisted and cambered wing.

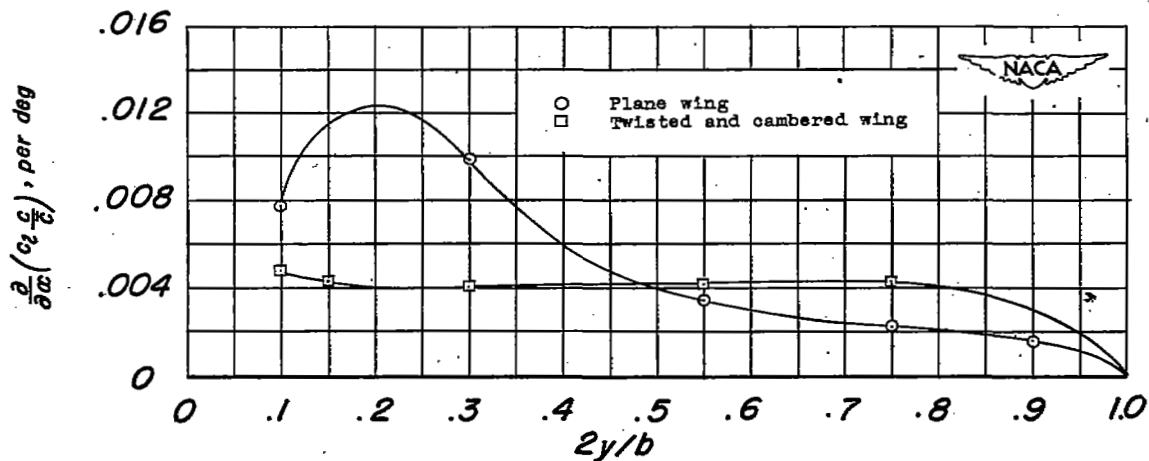


Figure 22.- Effects of twist and camber on the variations with angle of attack of the incremental loading due to the addition of the body.

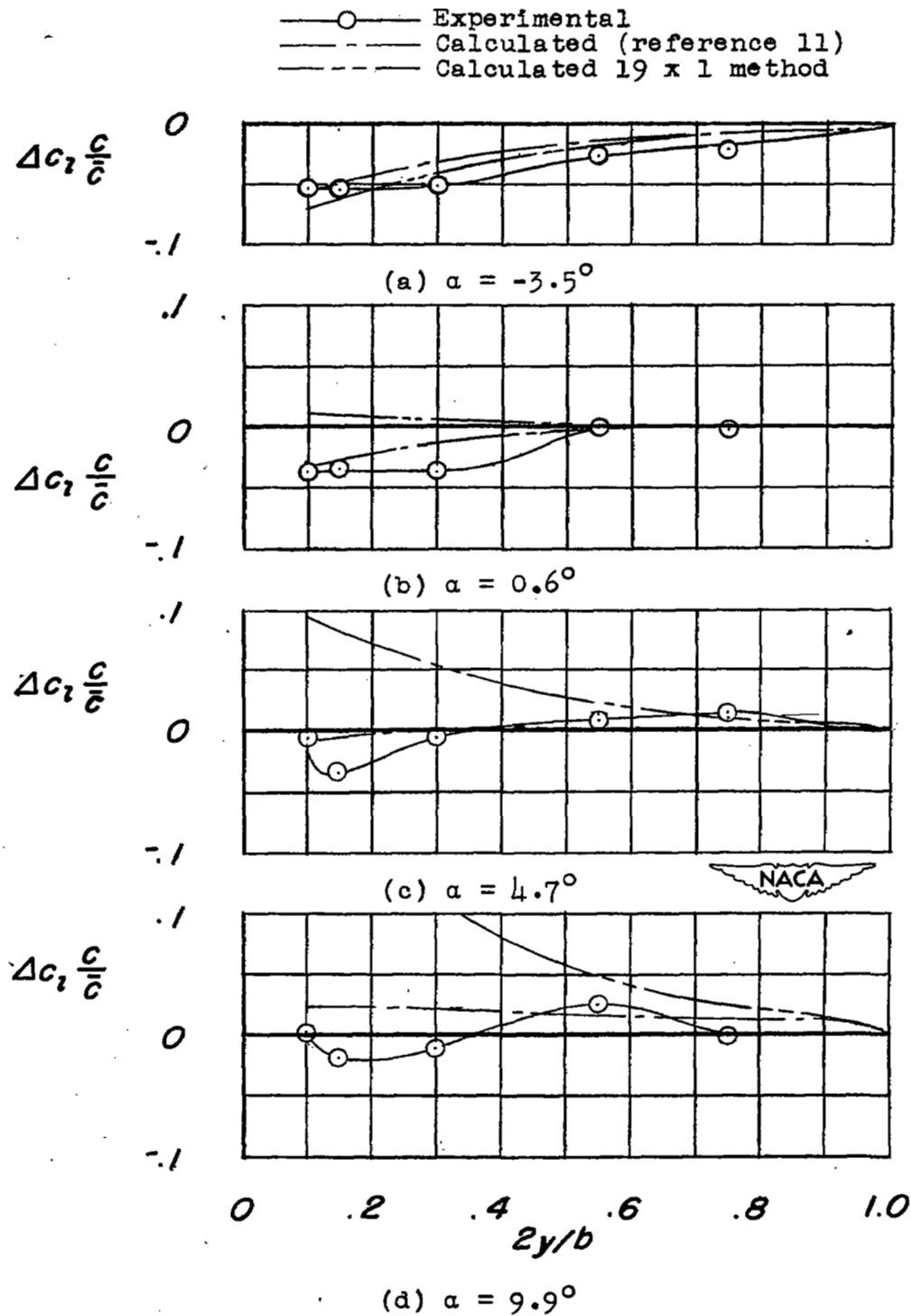


Figure 23.- Incremental load distributions due to the addition of a body to the twisted and cambered wing and comparisons with two calculated distributions. $i_w = 0^\circ$.

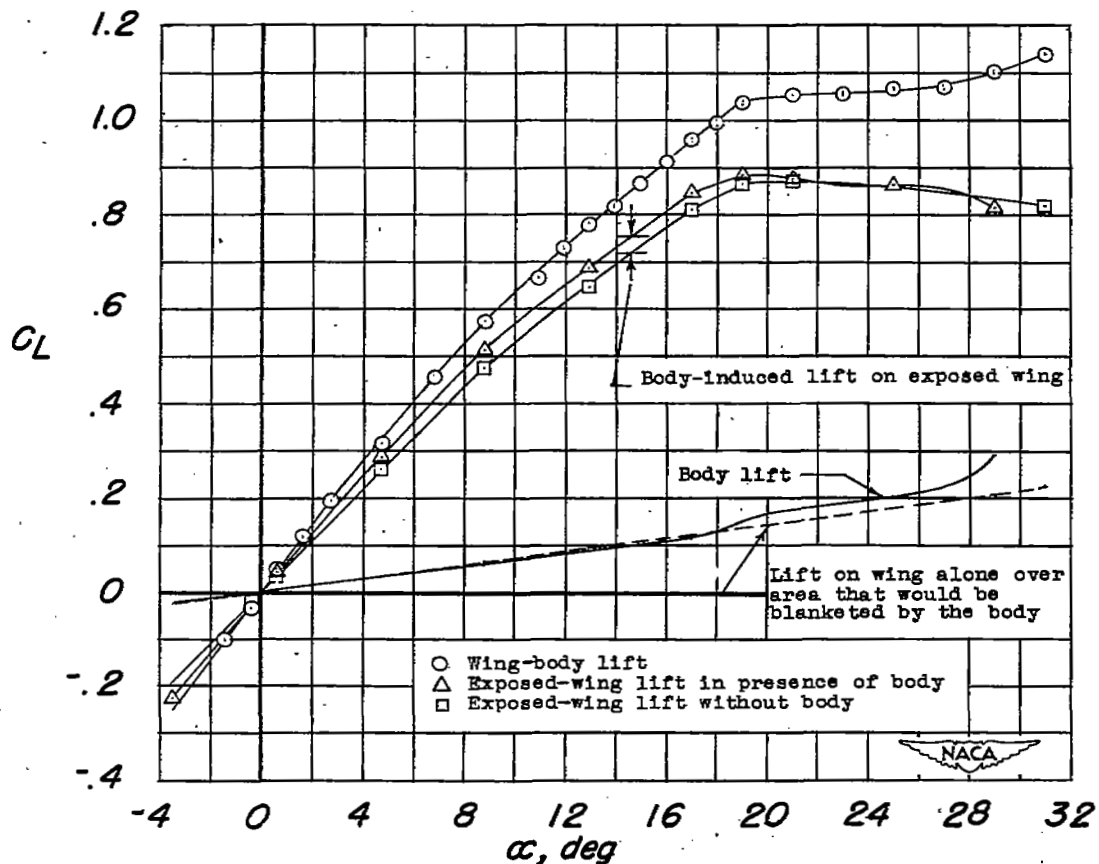


Figure 24.- The division of lift on the plane wing-body combination.
 $i_w = 0^\circ$.

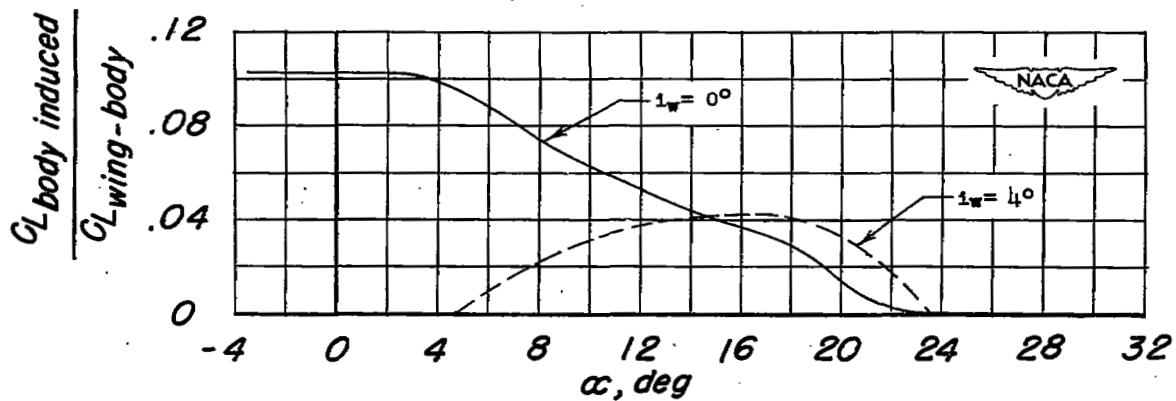
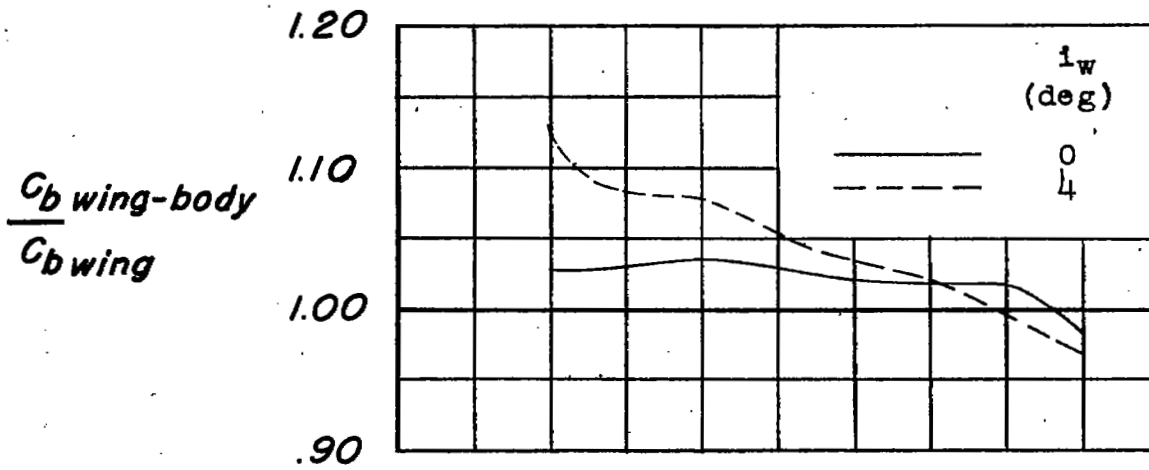
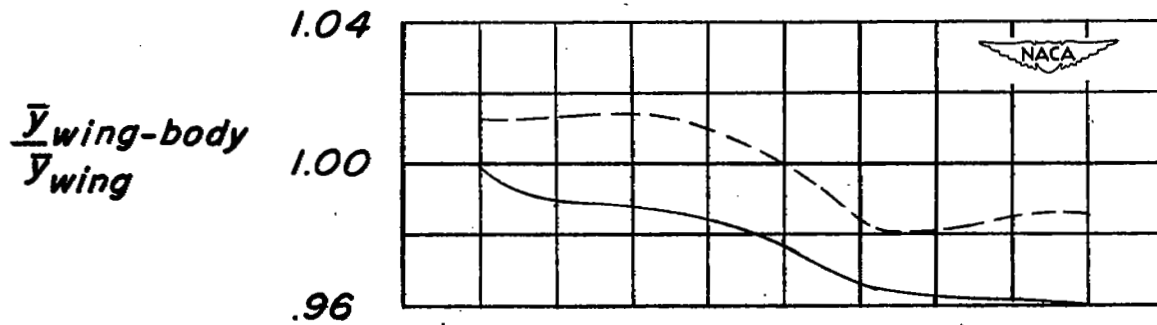


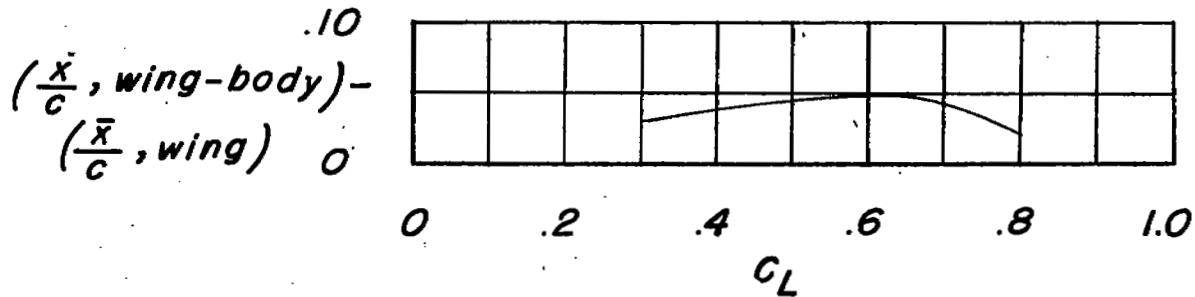
Figure 25.- Fraction of total lift of the plane wing-body combination that is induced by the body on the exposed wing.



(a) Wing-body juncture bending-moment coefficients.



(b) Lateral centers of pressure.



(c) Longitudinal centers of pressure.

Figure 26.- The effects of the body on the exposed plane wing characteristics, for two angles of incidence.

SECURITY INFORMATION

NASA Technical Library



3 1176 01437 5258

~~CONFIDENTIAL~~
UNCLASSIFIED